

Revisiting the luminosity and redshift distributions of long gamma-ray bursts

Guang-Xuan Lan,^{1,2} Jun-Jie Wei,^{1,2*} Hou-Dun Zeng,^{1,3†} Ye Li¹ and Xue-Feng Wu^{1,2‡}

¹Purple Mountain Observatory, Chinese Academy of Sciences, Nanjing 210023, China

²School of Astronomy and Space Science, University of Science and Technology of China, Hefei 230026, China

³Key Laboratory of Dark Matter and Space Astronomy Purple Mountain Observatory, Chinese Academy of Sciences Nanjing 210023, China

Accepted XXX. Received YYY; in original form ZZZ

ABSTRACT

In this work, we update and enlarge the long gamma-ray burst (GRB) sample detected by the *Swift* satellite. Given the incomplete sampling of the faint bursts and the low completeness in redshift measurement, we carefully select a subsample of bright *Swift* bursts to revisit the GRB luminosity function (LF) and redshift distribution by taking into account the probability of redshift measurement. Here we also explore two general expressions for the GRB LF, i.e., a broken power-law LF and a triple power-law LF. Our results suggest that a strong redshift evolution in luminosity (with an evolution index of $\delta = 1.92^{+0.25}_{-0.37}$) or in density ($\delta = 1.26^{+0.33}_{-0.34}$) is required in order to well account for the observations, independent of the assumed expression of the GRB LF. However, in a one-on-one comparison using the Akaike information criterion, the best-fitting evolution model involving the triple power-law LF is statistically preferred over the best-fitting one involving the broken power-law LF with a relative probability of $\sim 94.3\%$ versus $\sim 5.7\%$. Extrapolating our fitting results to the flux limit of the whole *Swift* sample, and considering the trigger probability of *Swift*/Burst Alert Telescope in detail, we find that the expectations from our evolution models provide a good representation of the observed distributions of the whole sample without the need for any adjustment of the model free parameters. This further confirms the reliability of our analysis results.

Key words: gamma-ray burst: general – stars: formation – methods: statistical

1 INTRODUCTION

Gamma-ray bursts (GRBs) are the most luminous explosive transients in the cosmos, which can be detected from our local universe up to extremely high redshifts (Salvaterra et al. 2009b; Tanvir et al. 2009; Cucchiara et al. 2011). Generally, long GRBs with durations $T_{90} > 2$ s are believed to be powered by the core collapse of massive stars (e.g., Woosley 1993; Paczyński 1998; Woosley & Bloom 2006), a perspective given strong support by observations of several long GRBs associated with supernovae (e.g., Hjorth et al. 2003; Stanek et al. 2003). The collapsar model suggests that the births of long GRBs should trace the cosmic star formation history (e.g., Totani 1997; Piran 2004; Zhang & Mészáros 2004; Zhang 2007), and long GRBs may therefore be excellent tools to probe the star formation rate (SFR) at high redshifts ($z \geq 4$; e.g., Chary et al. 2007; Yüksel et al. 2008;

Kistler et al. 2009; Wang & Dai 2009; Wang 2013; Wei et al. 2014).

In the past few years, the properties of the population of long GRBs and their evolution with cosmic time have been widely investigated by different authors (e.g., Porciani & Madau 2001; Lloyd-Ronning et al. 2002, 2019; Firmani et al. 2004; Guetta et al. 2005; Natarajan et al. 2005; Daigne et al. 2006; Guetta & Piran 2007; Le & Dermer 2007; Salvaterra & Chincarini 2007; Kistler et al. 2008; Salvaterra et al. 2009a, 2012; Butler et al. 2010; Campisi et al. 2010; Qin et al. 2010; Wanderman & Piran 2010; Cao et al. 2011; Virgili et al. 2011; Lu et al. 2012; Robertson & Ellis 2012; Tan et al. 2013; Wei et al. 2014; Petrosian et al. 2015; Tan & Wang 2015; Yu et al. 2015; Deng et al. 2016; Pescalli et al. 2016; Wei & Wu 2017; Paul 2018; Lan et al. 2019; Le et al. 2020; Dong et al. 2021; Palmerio & Daigne 2021). There is a general agreement on the fact that GRBs may have experienced some kind of evolution with redshift, whereas the nature and the level of such evolution are uncertain and still a matter of debate. It should be emphasized

* E-mail: jjwei@pmo.ac.cn (JJW)

† E-mail: zhd@pmo.ac.cn (ZHD)

‡ E-mail: xfwu@pmo.ac.cn (XFW)

that the evolution features of GRBs are inferred from the statistics of the observational samples. However, as is well known, the observational samples inevitably subject to various instrumental selection effects and observational biases (Bloom 2003). It is difficult to reveal the intrinsic distributions of long GRBs and their evolution features from these samples. For example, a faint GRB with peak flux slightly over the instrumental detection threshold would not always make a trigger. Incomplete sampling of the faint bursts is thus a ubiquitous problem in observations. In addition, although the number of measured GRB redshifts has increased considerably in the *Swift* era, the bursts with redshift determinations account for only $\sim 1/3$ of all GRBs detected by *Swift*/Burst Alert Telescope (BAT). The low completeness level in redshift measurement would lead to biases in shaping GRB redshift distribution (Fiore et al. 2007; Salvaterra et al. 2012). Therefore, the distributions of long GRBs through cosmic time can only be unbiasedly studied by using a complete sample that is capable of adequately representing this population (Salvaterra et al. 2012; Pescalli et al. 2016; Lan et al. 2019), or by using an incomplete sample but carefully taking into account various instrumental selection effects.

A few attempts have been made to construct a complete flux-limited sample of long GRBs. For instance, Salvaterra et al. (2012) defined a well-selected subsample of bright *Swift* GRBs, which is composed of 58 bursts with favorable observing conditions for redshift measurement as proposed in Jakobsson et al. (2006) and with 1-s peak photon flux $P \geq 2.6$ photons $\text{cm}^{-2} \text{s}^{-1}$. This sample, which is complete in peak flux by definition, after careful selection turned out to be also highly complete ($\sim 90\%$) in redshift (i.e., 52 out of 58 bursts have measured z). Pescalli et al. (2016) extended the complete sample of Salvaterra et al. (2012) with additional bursts that satisfy the same selection criteria. This extended sample contains 99 bursts, 81 of them with measured redshift and luminosity for a completeness level of $\sim 82\%$. Though the complete sample can provide a solid basis for the statistical study of the long-GRB population (Salvaterra et al. 2012; Pescalli et al. 2016; Lan et al. 2019), its current sample size is admittedly small. We have to acknowledge the statistical limitations of the study due to the small sample size. On the other hand, many previous works relied on the use of incomplete samples. Despite they have relatively large sample sizes (hundreds of bursts), the instrumental selection effects and possible observational biases have not been handled very well (Bryant et al. 2021).

In this work, we update and enlarge the GRB sample observed by *Swift*/BAT. Our principal goal in this paper is to make use of the latest incomplete sample to revisit the GRB luminosity function (LF) and redshift distribution by considering various instrumental selection effects, including the incomplete sampling of the faint bursts and the probability of redshift measurement. In order to examine our analysis method's effectiveness and reliability, we also extrapolate our findings to the detection limit of *Swift* by considering the trigger probability of *Swift*/BAT, and the result shows that our method is effective and reliable.

This paper is arranged as follows. In Section 2, we assemble our *Swift* GRB sample and estimate the probability of redshift measurement for a GRB. Our analysis method is described in Section 3, and the model results are pre-

sented in 4. In Section 5, we extrapolate our fitting results to the flux limit of the whole redshift sample with the trigger probability of *Swift*/BAT. Our conclusions are drawn in Section 6. Throughout this paper a flat Λ CDM cosmological model with $H_0 = 70 \text{ km s}^{-1} \text{ Mpc}^{-1}$, $\Omega_m = 0.3$, and $\Omega_\Lambda = 0.7$ is adopted.

2 SWIFT GRB SAMPLE AND REDSHIFT MEASUREMENT PROBABILITY

2.1 The sample

Since the launch of the *Swift* satellite on 2004 November (Gehrels et al. 2004), more than one thousand GRBs have been detected. Our sample is only limited to those long GRBs detected by *Swift*. This is because it is a homogeneous sample whose size is large enough to do a reliable statistical analysis. We collect long GRBs with durations $T_{90} > 2 \text{ s}$ up to 2019 November. Moreover, we require 1-s peak photon flux for analysis and it turns out to be 1111 GRBs. Figure 1 shows the peak-flux distribution of all the 1111 bursts, ranging from 0.04 to 331 photons $\text{cm}^{-2} \text{s}^{-1}$. Of these 1111, 429 bursts have accurate redshift measurements. The redshift completeness level is only $\sim 39\%$. We calculate the peak bolometric luminosities in the $1\text{--}10^4 \text{ keV}$ rest-frame energy range for those GRBs having redshifts (see specific formula in Sun et al. 2015). Within long GRBs, the low-luminosity GRBs (LLGRBs; $L < 10^{49} \text{ erg s}^{-1}$) have been claimed to be a distinct population (Soderberg et al. 2004; Cobb et al. 2006; Chapman et al. 2007; Liang et al. 2007). There are five bursts with $L < 10^{49} \text{ erg s}^{-1}$ in our redshift sample. The luminosity distribution of our sample shows that the LLGRBs are not the straightforward extension of high-luminosity GRBs (HLGRBs) to low luminosities. Compared to the first component of HLGRBs, the incline of LLGRBs is slightly steeper and their normalization is a little bit lower. Given the slight mismatch between LLGRBs and HLGRBs, we discard these five LLGRBs. We have verified that our results are only weakly sensitive to the abandon of five LLGRBs. The remaining 424 long GRBs with known redshifts are presented in Table A1 which includes the following information for each GRB: its name, the peak photon flux P in the observer frame *Swift*/BAT [15–150] keV energy band, the redshift z , the spectral parameters (low- and high-energy photon spectral indices α and β , and the observed peak energy E_p), and the peak bolometric luminosity L . The spectrum is a cut-off power law if only the low energy photon index α and the peak energy E_p are reported, and a Band function (Band et al. 1993) if the high energy photon index β is also given. For those GRBs without spectral information, we adopt the typical values of the Band spectrum ($\alpha = -1$, $\beta = -2.3$, and $E_p = 250 \text{ keV}$; Preece et al. 2000; Kaneko et al. 2006) to calculate L .

The *Swift*/BAT trigger is complicated and its sensitivity for GRBs is difficult to parametrize exactly (Band 2006). In practice, not all faint bursts with peak flux slightly over the instrument threshold would be triggered successfully. As shown in Figure 1, due to incomplete sampling of the faint bursts, the peak-flux distribution is significantly deviated from an ideal power law at the low end. Thus, given this incomplete sampling, the intrinsic peak-flux distribution is necessarily different from the observed one. A simple

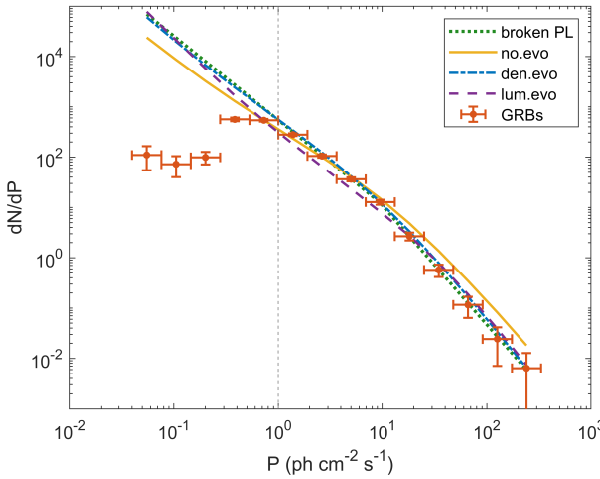


Figure 1. The peak-flux distribution of 1111 long GRBs detected by *Swift*/BAT. The vertical dotted line represents the limiting flux ($1 \text{ photons cm}^{-2} \text{ s}^{-1}$) above which the incomplete sampling of the faint bursts induced by the instrumental selection effect becomes negligible. The green dotted line shows the best-fitting result to the observed peak-flux distribution with $P \geq 1 \text{ photons cm}^{-2} \text{ s}^{-1}$ by using a broken power-law function. Other curves show the expected flux distributions from different best-fitting models with the assumed triple power-law LF: no evolution model (orange solid line), density evolution model (blue dot-dashed line), and luminosity evolution model (purple dashed line).

approach to recovering the intrinsic peak-flux distribution is obtained by studying the sample above $P \approx 1 \text{ photons cm}^{-2} \text{ s}^{-1}$. Indeed, above this flux limit, the instrumental selection effect affecting the incomplete sampling is negligible (see Figure 1). Thus, we define a sharp trigger threshold: the trigger probability θ_γ of bursts with $P \geq 1 \text{ photons cm}^{-2} \text{ s}^{-1}$ is 100%. Above the flux limit ($P_{\text{lim}} = 1 \text{ photons cm}^{-2} \text{ s}^{-1}$), BAT detects 733 GRBs. 302 of them have measured redshift so that the redshift completeness level is slightly increased to $\sim 41\%$. Still, this level of completeness is far too low to permit reliable population studies. Thus, the sample of the 302 GRBs with $P \geq 1 \text{ photons cm}^{-2} \text{ s}^{-1}$ will be used to construct the GRB LF and its evolution with cosmic time by considering the probability for redshift measurement.

2.2 Redshift measurement probability

The low completeness in redshift may disguise the intrinsic redshift distribution of GRBs (Fiore et al. 2007; Salvaterra et al. 2012). In order to mitigate the incompleteness problem, we empirically model probability of redshift measurement for a *Swift* detected GRB. Actually, the redshift measurement is quite complex, depending on several artificial effects, such as the optical follow-up observation, spectral line confirmation, and so on (Bloom 2003). It is difficult to model favorable observing conditions for the optical follow-up searches. But Band (2006) suggested that the probability to measure a redshift could still be empirically modeled, and it should be a function of the burst flux, duration, and other factors. We restrict ourselves here only to the dependence of the probability on the peak flux, since this is the observed quantity we adopt for the analysis in this paper. Indeed, observations suggest redshifts are preferentially

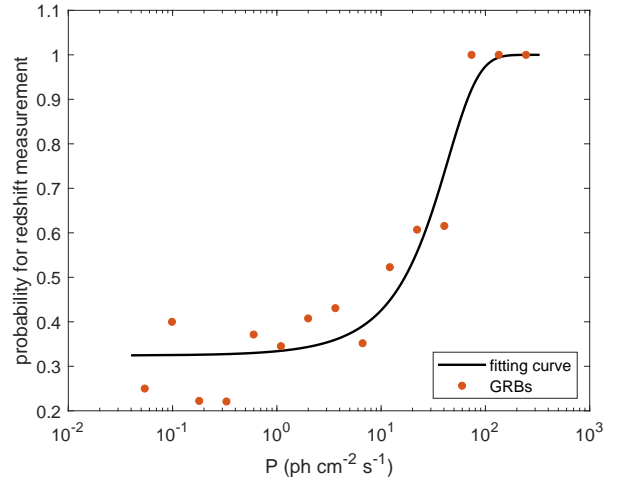


Figure 2. Redshift measurement probability as a function of the peak photon flux for *Swift* long GRBs. The best-fitting curve is parametrized in equation (1).

measured for brighter GRBs. Figure 2 shows the redshift measurement probability θ_z as a function of the peak flux P , in which the probabilities are estimated by the fraction of the number of bursts with redshift measurement in each bin to the overall number of detected bursts in the corresponding bin. It is clear that the probability of redshift determination for the burst in our sample is mildly related to P , reflecting the observational fact that the probability increases with increasing P values. Here we use an empirical function to model the redshift measurement probability

$$\theta_z(P) = \frac{1}{1 + \xi_z \kappa_z^P}, \quad (1)$$

where the best-fitting parameters are $\xi_z = 2.09 \pm 0.26$ and $\kappa_z = 0.96 \pm 0.01$ at 68% confidence level.

3 ANALYSIS METHOD

A maximum likelihood method firstly introduced by Marshall et al. (1983) is adopted in our analysis. The model free parameters can be optimized by maximizing the likelihood function (e.g., Chiang & Mukherjee 1998; Narumoto & Totani 2006; Ajello et al. 2009, 2012; Abdo et al. 2010; Zeng et al. 2014, 2016; Lan et al. 2019; Qu et al. 2019), i.e.,

$$\mathcal{L} = \exp(-N_{\text{exp}}) \prod_{i=1}^{N_{\text{obs}}} \Phi(L_i, z_i, t_i), \quad (2)$$

where N_{exp} denotes the expected number of GRB detections, N_{obs} represents the observed number of the sample, and $\Phi(L, z, t)$ is the observed rate of bursts per unit time at redshift $z \sim z + dz$ with luminosity $L \sim L + dL$, which is given by

$$\begin{aligned} \Phi(L, z, t) &= \frac{d^3 N}{dtdzdL} = \frac{d^3 N}{dtdVdL} \times \frac{dV}{dz} \\ &= \frac{\Delta\Omega}{4\pi} \theta(P) \frac{\psi(z)}{1+z} \phi(L, z) \times \frac{dV}{dz}, \end{aligned} \quad (3)$$

where $\Delta\Omega = 1.33 \text{ sr}$ is the *Swift*/BAT field of view, $\theta(P) \equiv \theta_\gamma(P)\theta_z(P)$ is the detection efficiency which represents the

probability to trigger and measure redshift for a burst with peak flux P , $\psi(z)$ is the comoving event rate of GRBs (in units of $\text{Mpc}^{-3} \text{ yr}^{-1}$) as a function of z , $(1+z)^{-1}$ reflects the cosmological time dilation, $\phi(L, z)$ is the normalized GRB LF which whether evolves with redshift dependents on the assumed model (see more below), and $dV(z)/dz = 4\pi c D_L^2(z)/[H_0(1+z)^2 \sqrt{\Omega_m(1+z)^3 + \Omega_\Lambda}]$ is the comoving volume element in a flat ΛCDM model. The $D_L(z)$ is the luminosity distance at z .

Within the context of the collapsar origin, the formation of each GRB just means the death of a short-lived massive star. Thus, the GRB formation rate $\psi(z)$ should in principle be connected to the cosmic SFR $\psi_*(z)$, i.e.,

$$\psi(z) = \eta \psi_*(z), \quad (4)$$

where η is the GRB formation efficiency that accounts for the number of GRBs formed per solar mass in stars and has units of M_\odot^{-1} . The SFR $\psi_*(z)$ (in units of $\text{M}_\odot \text{ yr}^{-1} \text{ Mpc}^{-3}$) can be expressed approximately by (Hopkins & Beacom 2006; Li 2008)

$$\psi_*(z) = \frac{0.0157 + 0.118z}{1 + (z/3.23)^{4.66}}. \quad (5)$$

For the GRB LF $\phi(L, z)$, we use the general expression in term of a broken power law:

$$\phi(L, z) = \frac{A}{\ln(10)L} \begin{cases} \left(\frac{L}{L_c(z)}\right)^a; & L \leq L_c(z), \\ \left(\frac{L}{L_c(z)}\right)^b; & L > L_c(z), \end{cases} \quad (6)$$

where A is a normalization constant, and a and b are the power-law indices before and after the break luminosity L_c . If the broken power-law model does not reproduce the data well, we introduce a triple power-law form, i.e.,

$$\phi(L, z) = \frac{A}{\ln(10)L} \begin{cases} \left(\frac{L}{L_{c_1}(z)}\right)^a; & L \leq L_{c_1}(z), \\ \left(\frac{L}{L_{c_1}(z)}\right)^b; & L_{c_1}(z) < L \leq L_{c_2}(z), \\ \left(\frac{L_{c_2}(z)}{L_{c_1}(z)}\right)^b \left(\frac{L}{L_{c_2}(z)}\right)^c; & L > L_{c_2}(z), \end{cases} \quad (7)$$

where a , b , and c are the power-law indices for three segments, and L_{c_1} and L_{c_2} are the two break luminosities.

Considering the flux threshold that used to define 100-percent trigger (i.e., $P_{\lim} = 1 \text{ photons cm}^{-2} \text{ s}^{-1}$ in the 15–150 keV energy band), the expected number of GRBs can be expressed as

$$N_{\exp} = \frac{\Delta\Omega T}{4\pi} \int_0^{z_{\max}} \int_{\max[L_{\min}, L_{\lim}(z)]}^{L_{\max}} \theta(P(L, z)) \frac{\psi(z)}{1+z} \times \phi(L, z) dL dV(z). \quad (8)$$

where $T \sim 15 \text{ yr}$ is the time of activity of *Swift* that covers our sample. Since $z < 10$ for the current BAT sample, the maximum redshift for our analysis is $z_{\max} = 10$. The luminosity function is assumed to extend from $L_{\min} = 10^{49} \text{ erg s}^{-1}$ to $L_{\max} = 10^{55} \text{ erg s}^{-1}$ (Pescalli et al. 2015). The luminosity threshold appearing in Equation (8) can be estimated through

$$L_{\lim}(z) = 4\pi D_L^2(z) P_{\lim} \frac{\int_{1/(1+z) \text{ keV}}^{10^4/(1+z) \text{ keV}} EN(E) dE}{\int_{15 \text{ keV}}^{150 \text{ keV}} N(E) dE}, \quad (9)$$

where $N(E)$ is the GRB photon spectrum. We adopt a

typical Band function spectrum with low- and high-energy spectral indices -1 and -2.3 , respectively (Band et al. 1993; Preece et al. 2000; Kaneko et al. 2006). In order to broadly estimate the spectral peak energy E_p for a given L , we assume the validity of the empirical E_p - L correlation (Yonetoku et al. 2004; Nava et al. 2012), i.e., $\log [E_p(1+z)] = -25.33 + 0.53 \log L$.

Due to the fact that (i) the connection between the GRB formation rate and the cosmic SFR may not be unbiased and (ii) the GRB LF may evolve with redshift, we introduce an extra evolving factor $(1+z)^\delta$ in our above equations, where δ is an (unknown) evolution parameter. We consider three different models. In the first model, the GRB formation rate purely follows the SFR, i.e., $\psi(z) = \eta \psi_*(z)$, and the LF does not evolve with redshift, i.e., $L_{c_i}(z) = L_{c_i,0} = \text{constant}$. In the second one, while the GRB formation rate is still proportional to the SFR, the break luminosity in the GRB LF increases with redshift as $L_{c_i}(z) = L_{c_i,0}(1+z)^\delta$. Finally, we consider a model in which the formation rate follows the SFR in conjunction with an extra evolving factor, i.e., $\psi(z) = \eta \psi_*(z)(1+z)^\delta$, and the LF is taken to be non-evolving.

For a given model, the free parameters can be optimized by maximizing the likelihood function (Equation (2)). Since there are multiple parameters in our various models, the Markov Chain Monte Carlo (MCMC) sampling technology is employed to derive the best-fitting values and the associated 1σ uncertainties for the model parameters. We adopt the MCMC code from GWMC,¹ which is an implementation of the Goodman and Weare 2010 Affine invariant ensemble MCMC sampler (Goodman & Weare 2010; Foreman-Mackey et al. 2013).

4 RESULTS

Using the above analysis method, we can optimize the values of the model free parameters, including the GRB LF, the evolution parameter, and the GRB formation efficiency η . The best-fitting parameters and their corresponding 1σ confidence level for different models are given in Table 1. To determine statistically which of the models is preferred by the observational data, we also report the log-likelihood value $\ln \mathcal{L}$ and the Akaike Information Criterion (AIC) score in the last two columns of Table 1. For each fitted model, the AIC score is evaluated as $\text{AIC} = -2 \ln \mathcal{L} + 2n$, where n is the number of free parameters (Akaike 1974; Liddle 2007). With AIC_i characterizing model \mathcal{M}_i , the unnormalized confidence that this model is correct is the Akaike weight $\exp(-\text{AIC}_i/2)$. Informally, \mathcal{M}_i has the relative probability

$$P(\mathcal{M}_i) = \frac{\exp(-\text{AIC}_i/2)}{\exp(-\text{AIC}_1/2) + \exp(-\text{AIC}_2/2)} \quad (10)$$

of being the true model in a one-on-one comparison. Thus, the difference $\text{AIC}_2 - \text{AIC}_1$ determines the extent to which \mathcal{M}_1 is preferred over \mathcal{M}_2 .

The redshift and luminosity distributions of 302 GRBs with $P \geq 1 \text{ photons cm}^{-2} \text{ s}^{-1}$ are shown in Figure 3 as well as in Figure 4. We test for each model the two different

¹ <https://github.com/grinsted/gwmc>

Table 1. Best-fitting parameters for different models.

Model	Evolution parameter	η ($10^{-8} M_{\odot}^{-1}$)	a	b	c	$\log L_c$ (erg s $^{-1}$)	$\ln \mathcal{L}$	AIC
Broken power-law luminosity function								
No evolution	...	$5.21^{+0.91}_{-0.95}$	$-0.38^{+0.04}_{-0.04}$	$-1.63^{+0.26}_{-0.26}$...	$52.90^{+0.10}_{-0.10}$	-70.15	148.30
Luminosity evolution	$\delta = 1.85^{+0.24}_{-0.23}$	$3.58^{+0.73}_{-0.80}$	$-0.46^{+0.08}_{-0.08}$	$-1.30^{+0.18}_{-0.15}$...	$51.62^{+0.19}_{-0.20}$	-42.08	94.16
Density evolution	$\delta = 1.43^{+0.22}_{-0.20}$	$3.79^{+0.80}_{-0.75}$	$-0.60^{+0.05}_{-0.05}$	$-1.65^{+0.27}_{-0.28}$...	$52.98^{+0.11}_{-0.12}$	-43.63	97.26
Triple power-law luminosity function								
No evolution	...	$15.45^{+7.79}_{-7.65}$	$-1.62^{+0.73}_{-0.69}$	$-0.35^{+0.04}_{-0.04}$	$-1.65^{+0.24}_{-0.26}$	$49.99^{+0.35}_{-0.42}, 52.92^{+0.09}_{-0.10}$	-67.06	146.12
Luminosity evolution	$\delta = 1.92^{+0.25}_{-0.37}$	$9.59^{+4.71}_{-4.15}$	$-1.40^{+0.55}_{-0.62}$	$-0.25^{+0.12}_{-0.13}$	$-1.17^{+0.08}_{-0.29}$	$50.16^{+0.37}_{-0.42}, 51.61^{+0.15}_{-0.29}$	-37.27	88.54
Density evolution	$\delta = 1.26^{+0.33}_{-0.34}$	$8.50^{+3.65}_{-3.68}$	$-0.97^{+0.19}_{-0.24}$	$-0.49^{+0.09}_{-0.08}$	$-1.64^{+0.26}_{-0.25}$	$50.55^{+0.20}_{-0.21}, 52.92^{+0.11}_{-0.11}$	-40.68	95.36

Note. Parameter values were computed as the medians of the best-fitting parameters to the Monte Carlo sample. Errors show the 68% containment regions around the median values

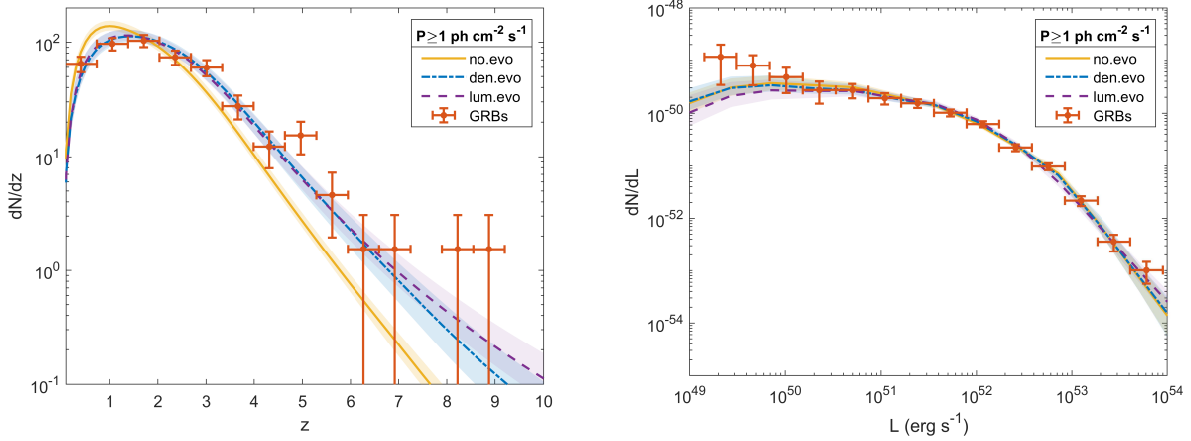


Figure 3. Redshift and luminosity distributions of 302 *Swift* GRBs with $P \geq 1$ photons cm $^{-2}$ s $^{-1}$ (the solid points, with the number of detection in each redshift or luminosity bin indicated by a red point with Poisson error bars). Different curves correspond to the expected distributions from different best-fitting models: no evolution model (orange solid lines), density evolution model (blue dot-dashed lines), and luminosity evolution model (purple dashed lines). Shadow regions represent the 1σ confidence regions of the corresponding models. In all models, the broken power-law LF has been assumed.

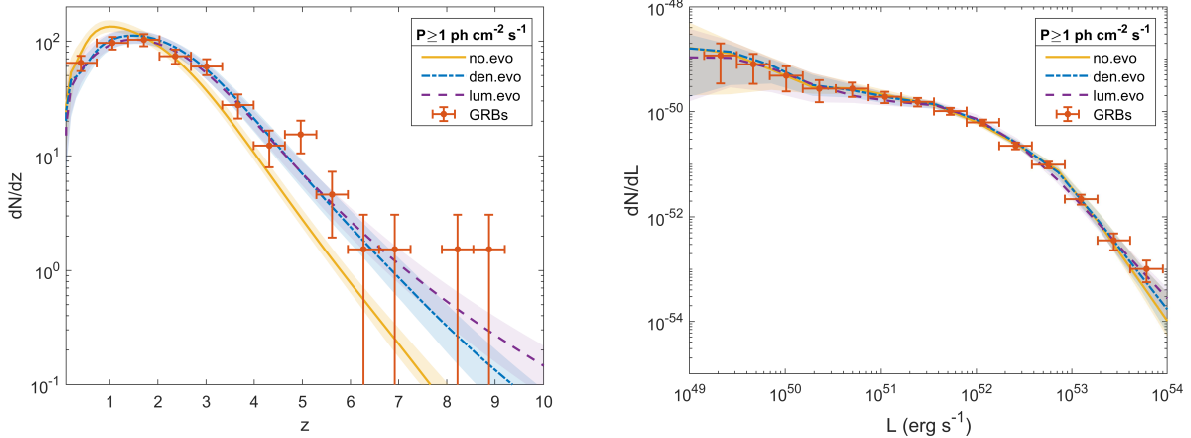


Figure 4. Same as Figure 3, except now for the scenario with the assumed triple power-law LF.

GRB LF expressions described in Section 3, and we display in Figure 3 the best-fitting results of different models with the broken power-law LF and in Figure 4 the results with the triple power-law LF.

4.1 No evolution model

In the no evolution model, we assume that long GRBs strictly adhere to the star formation history and that their LF does not evolve with redshift ($L_c(z) = L_{c,0} = \text{constant}$). Figure 3 shows the expected z and L distributions for different models with the assumed broken power-law LF. It is clear that the expectation from the no evolution model (orange solid lines) does not provide a good description of the observed distributions of our sample. Particularly, the peak of the expected z distribution appears at a lower redshift than observed, and both the rate of GRBs at high- z and the L distribution at the low end are underestimated. On the basis of the AIC model selection criterion, we can safely exclude this model as having a probability of only $\sim 10^{-12}$ of being correct compared to the luminosity evolution model with the assumed broken power-law LF.

Figure 4 is same as Figure 3, but with the assumed triple power-law LF. The results of our fitting from the no evolution model are indicated with orange solid lines. Although the fit of the L distribution now looks good, the expected z distribution from this model again is incompatible with the observation. According to the AIC model selection criterion, we confirm that the no evolution model can be discarded as having a probability of only $\sim 10^{-13}$ of being correct compared to the luminosity evolution model with the assumed triple power-law LF.

4.2 Luminosity evolution model

An evolving GRB LF can lead to enhanced detection of GRBs at high- z . In this model, the GRB formation rate still follows the cosmic SFR, but the break luminosity of the GRB LF is assumed to be evolving with redshift as $L_c(z) = L_{c,0}(1+z)^\delta$. That is, high- z GRBs are assumed to be brighter than low- z bursts. With the broken power-law LF, we find that a strong luminosity evolution with $\delta = 1.85^{+0.24}_{-0.23}$ reproduces the observed z and L distributions (purple dashed lines in Figure 3) quite well. However, we note that the broken power-law LF tends to underestimate the number of low- L bursts with respect to the observed one.

For the case with the assumed triple power-law LF, both the two break luminosities increase with redshift as $L_{c1}(z) = L_{c1,0}(1+z)^\delta$ and $L_{c2}(z) = L_{c2,0}(1+z)^\delta$. We find that a strong luminosity evolution with $\delta = 1.92^{+0.25}_{-0.37}$ is required to reproduce the observed z and L distributions (purple dashed lines in Figure 4) well. The required evolutionary effect does not depend on the assumed expression of the GRB LF. However, the AIC shows that the probability of the luminosity evolution model with the triple power-law LF being correct is $\sim 94.3\%$ compared to the same evolution model but with the broken power-law LF examined above. Note that Sun et al. (2015) also found that the GRB LF is best characterized as a triple power law.

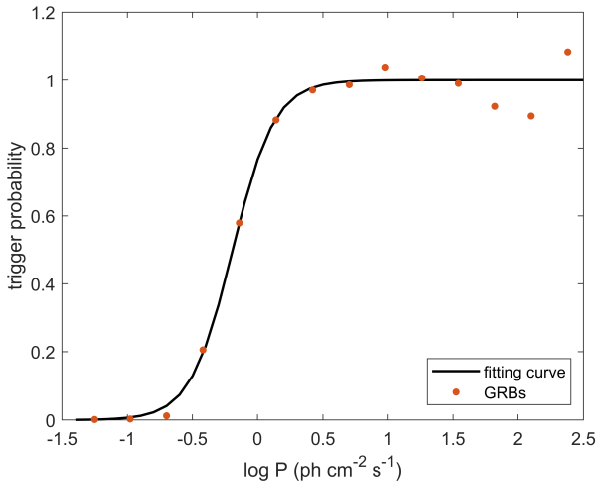


Figure 5. Trigger probability as a function of the peak flux for *Swift* long GRBs. The best-fitting curve is parametrized in equation (13).

4.3 Density evolution model

An increase of the GRB formation rate with redshift can also enhance the high- z GRB detection. In this model, the break luminosity in the GRB LF is constant, but the GRB rate is proportional to the cosmic SFR with an additional evolution parameterized by $(1+z)^\delta$, i.e., $\psi(z) = \eta\psi_*(z)(1+z)^\delta$. With the broken power-law LF, we find that a strong density evolution with $\delta = 1.43^{+0.22}_{-0.20}$ fits the observations best (blue dot-dashed lines in Figure 3), even though there are still some minor flaws in the fit of low luminosities.

For the case with the assumed triple power-law LF, the best fit is produced with a density evolution with $\delta = 1.26^{+0.33}_{-0.34}$. This model is represented by the blue dot-dashed lines in Figure 4. Obviously, the amount of evolution is independent of the assumed expression of the GRB LF. According to the AIC, the density evolution model with the triple power-law LF is slightly favoured compared to the same evolution model with the broken power-law LF, but the differences are statistically insignificant ($\sim 61.3\%$ for the former versus $\sim 38.7\%$ for the latter).

5 EXTRAPOLATE TO WHOLE SAMPLE WITH TRIGGER PROBABILITY

The total redshift sample presented in Table A1 comprises 424 long GRBs. However, due to incomplete sampling of the faint bursts, only 302 relatively bright bursts with $P \geq 1$ photons $\text{cm}^{-2} \text{s}^{-1}$ have been used in our analysis. A simple hard cutoff of the trigger threshold, $P_{\lim} = 1$ photons $\text{cm}^{-2} \text{s}^{-1}$, has also been assumed, i.e., 100% trigger of bursts with $P \geq P_{\lim}$. With the inclusion of the other 122 faint bursts with $0.04 \leq P < 1$ photons $\text{cm}^{-2} \text{s}^{-1}$, a more accurate and detailed description of the trigger efficiency θ_γ of *Swift/BAT* has to be considered in studying the properties of the long-GRB population. As Abdo et al. (2010) did in their treatment, we estimate the trigger probability of *Swift/BAT*

through

$$\theta_\gamma(P) = \frac{(dN/dP)_{\text{obs}}}{(dN/dP)_{\text{int}}}, \quad (11)$$

where $(dN/dP)_{\text{obs}}$ is the differential distribution of the observed peak flux (see data points in Figure 1) and $(dN/dP)_{\text{int}}$ is the intrinsic peak-flux distribution. As explained in Section 2.1, an approach to recovering the intrinsic peak-flux distribution is obtained by studying the sample above $P \approx 1$ photons $\text{cm}^{-2} \text{ s}^{-1}$. In order to parameterize the intrinsic peak-flux distribution, we perform a χ^2 fit to the differential data with $P \geq 1$ photons $\text{cm}^{-2} \text{ s}^{-1}$ using a broken power-law function:

$$\frac{dN}{dP} \propto \begin{cases} P^{\beta_1}; & P \leq P_c, \\ P_c^{\beta_1 - \beta_2} P^{\beta_2}; & P > P_c, \end{cases} \quad (12)$$

where β_1 and β_2 are the power-law indices before and after the break flux P_c . The best-fitting broken power-law model with parameters $\beta_1 = -1.67^{+0.05}_{-0.52}$, $\beta_2 = -2.37^{+0.72}_{-0.28}$, and $P_c = 9.24^{+194.76}_{-0.90}$ photons $\text{cm}^{-2} \text{ s}^{-1}$ is denoted by the green dotted line in Figure 1. Figure 1 also shows the expected flux distributions from different best-fitting models with the assumed triple power-law LF. Unsurprisingly, the reproduction of the P distribution from the no evolution model (orange solid line) is not as good as those from the luminosity evolution model (purple dashed line) or density evolution model (blue dot-dashed line). While, the best-fitting broken power-law model is in good agreement with the expectations from both the luminosity and density evolution models, implying that the evaluated $(dN/dP)_{\text{int}}$ from the broken power-law model provides a good description of the intrinsic peak-flux distribution. Extrapolating the evaluated $(dN/dP)_{\text{int}}$ to low P ($P < 1$ photons $\text{cm}^{-2} \text{ s}^{-1}$), we then estimate the trigger probability $\theta_\gamma(P)$ through Equation (11). The result is shown in Figure 5. θ_γ as a function of $\log(P)$ can be parametrized by a sigmoid function:

$$\theta_\gamma(P) = \frac{1}{1 + \exp(\xi_P \log P + \kappa_P)}, \quad (13)$$

where the best-fitting parameters are $\xi_P = -6.20 \pm 0.91$ and $\kappa_P = -1.18 \pm 0.24$ at 68% confidence level.

With the evaluated trigger probability of *Swift/BAT* (Equation (13)), we then compute the z and L distributions expected for the whole *Swift* redshift sample (424 bursts), by assuming a photon flux limit of $P_{\text{lim}} = 0.04$ photons $\text{cm}^{-2} \text{ s}^{-1}$ and fixing the model free parameters to the values given in Table 1 (entries 4–6, corresponding to the case with the assumed triple power-law LF). The results are shown in Figure 6 for the different evolution models explored here. The models are compared with the z and L distributions inferred from the whole redshift sample of GRBs detected by *Swift*. This whole sample has a redshift completeness level similar to our flux-cut sample but is larger in size and covers a broader flux range. We find that the expectations from our evolution models offer a good representation of the observed z and L distributions of the whole sample without the need for any adjustment of the model free parameters, whereas the no evolution model gives a poor match. This further supports the reliability of our analysis and sharpens the strength of our conclusions.

6 CONCLUSIONS

In this work, we update and enlarge the long GRB sample detected by the *Swift* satellite. The enlarged sample contains 1111 GRBs up to 2019 November, among which 424 bursts have measured redshift. Given the incomplete sampling of the faint bursts, we restrict ourselves to GRBs that are relatively bright in the 15–150 keV *Swift/BAT* energy band. In practice, we select bursts having 1-s peak photon flux $P \geq 1$ photons $\text{cm}^{-2} \text{ s}^{-1}$. Above this flux limit, the incomplete flux sampling induced by the instrumental selection effect becomes negligible. Our subsample is then composed of 733 GRBs with $P \geq 1$ photons $\text{cm}^{-2} \text{ s}^{-1}$, 302 of them with known redshifts for a completeness level of 41%. Given the low completeness level in redshift measurement, we model the redshift measurement probability based on the current *Swift* GRB sample.

Using the flux-limited GRB subsample, we construct the GRB LF and redshift distribution in the frameworks of different evolution models by taking into account the redshift measurement probability. The maximum likelihood algorithm is applied to perform an analysis for the redshift and luminosity distributions of the GRB sample, and the MCMC technology is applied to obtain the best-fitting parameters in each model. We find that GRBs must have experienced some sort of evolution with redshift, being more luminous or more numerous in the past than present day. In order to reproduce the observed distributions well, the burst luminosity should increase to $(1+z)^{1.92^{+0.25}_{-0.37}}$ or the GRB rate density should rise to $(1+z)^{1.26^{+0.33}_{-0.34}}$ with respect to the known cosmic evolution of the SFR, confirming previous findings derived from the similar parametric studies (e.g., Salvaterra et al. 2012; Lan et al. 2019). Besides these parametric studies, the non-parametric statistical method proposed by Lynden-Bell (1971) and Efron & Petrosian (1992) has also been widely used to determine the evolution of the GRB LF (e.g., Lloyd-Ronning et al. 2002; Petrosian et al. 2015; Yu et al. 2015; Pescalli et al. 2016). To our knowledge, the first attempt to determine the GRB luminosity evolution through the non-parametric method was presented in Lloyd-Ronning et al. (2002). We would like to stress that if we focus on the luminosity evolution model, our derived evolution index ($\delta = 1.92^{+0.25}_{-0.37}$) is broadly consistent with previous results based on the non-parametric studies: $\delta = 1.4 \pm 0.5$ by Lloyd-Ronning et al. (2002), $\delta = 2.3 \pm 0.8$ by Petrosian et al. (2015), $\delta = 2.43^{+0.41}_{-0.38}$ by Yu et al. (2015), and $\delta \sim 2.5$ by Pescalli et al. (2016).

We also explore two general expressions for the GRB LF: a broken power-law LF and a triple power-law LF. We find that the required evolutionary effect does not depend on the assumed GRB LF expression. However, in a one-on-one comparison using the AIC model selection criterion, the luminosity evolution model involving the triple power-law LF is statistically preferred over the same model but involving the broken power-law LF with a relative probability of $\sim 94.3\%$ versus $\sim 5.7\%$. Sun et al. (2015) also suggested that a triple power-law expression can give the best description for the GRB LF.

Extrapolating our fitting results to the flux limit ($P = 0.04$ photons $\text{cm}^{-2} \text{ s}^{-1}$) of the whole *Swift* redshift sample, and considering the trigger probability of *Swift/BAT* in detail, we find that the expectations from our luminosity and

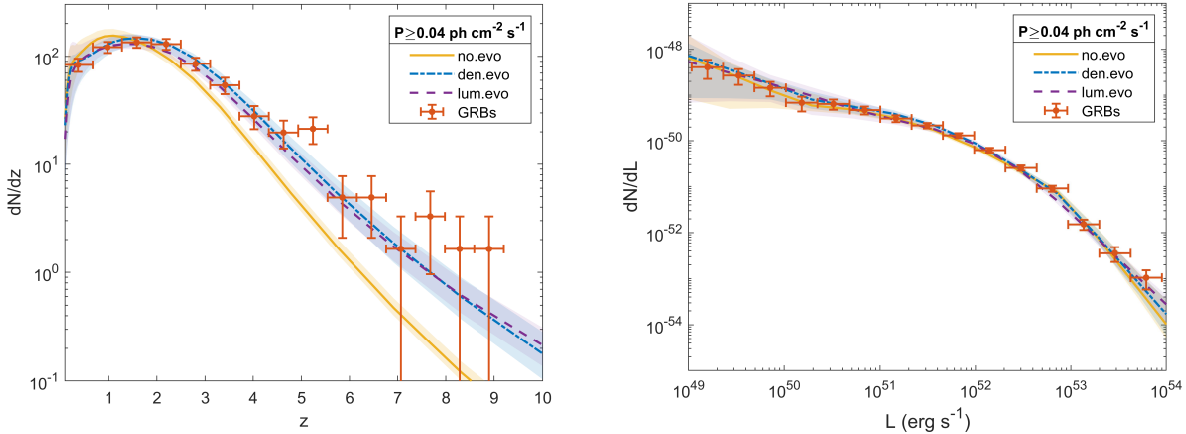


Figure 6. Redshift and luminosity distributions of the whole *Swift* sample (424 GRBs with $P \geq 0.04$ photons $\text{cm}^{-2} \text{s}^{-1}$). Model results are shown as in Figure 4, but now with the inclusion of the trigger probability of *Swift*/BAT (Equation (13)). There has no attempt to fit the observed redshift and luminosity distributions.

density evolution models are well consistent with the observations of the whole sample without the requirement for any adjustment of the model free parameters. This further confirms that our analysis results are reliable. We also note that since the two evolution models explored here predict very similar distributions, it is difficult to distinguish between luminosity and density evolution only on the basis of the current *Swift* sample.

ACKNOWLEDGEMENTS

We are grateful to the anonymous referee for insightful comments. This work is partially supported by the National Natural Science Foundation of China (grant Nos. 11725314, U1831122, 12041306 and 11703094), the Youth Innovation Promotion Association (2017366), the Key Research Program of Frontier Sciences (grant No. ZDBS-LY-7014) of Chinese Academy of Sciences, and the Major Science and Technology Project of Qinghai Province (2019-ZJ-A10).

DATA AVAILABILITY

The data underlying this article will be shared on reasonable request to the corresponding author.

REFERENCES

- Abdo A. A., et al., 2010, *ApJ*, **720**, 435
 Ajello M., et al., 2009, *ApJ*, **699**, 603
 Ajello M., et al., 2012, *ApJ*, **751**, 108
 Akaike H., 1974, *IEEE Transactions on Automatic Control*, **19**, 716
 Band D. L., 2006, *ApJ*, **644**, 378
 Band D., et al., 1993, *ApJ*, **413**, 281
 Bissaldi E., Meegan C., 2017, GRB Coordinates Network, **21297**, 1
 Bissaldi E., Hui C. M., Connaughton V., Hamburg R., 2016, GRB Coordinates Network, **19769**, 1
 Bissaldi E., Veres P., Fermi GBM Team 2019, GRB Coordinates Network, **26000**, 1
 Bloom J. S., 2003, *AJ*, **125**, 2865
 Bryant C. M., Osborne J. A., Shahmoradi A., 2021, *MNRAS*, **504**, 4192
 Butler N. R., Kocevski D., Bloom J. S., Curtis J. L., 2007, *ApJ*, **671**, 656
 Butler N. R., Bloom J. S., Poznanski D., 2010, *ApJ*, **711**, 495
 Campisi M. A., Li L.-X., Jakobsson P., 2010, *MNRAS*, **407**, 1972
 Cao X.-F., Yu Y.-W., Cheng K. S., Zheng X.-P., 2011, *MNRAS*, **416**, 2174
 Chapman R., Tavir N. R., Priddey R. S., Levan A. J., 2007, *MNRAS*, **382**, L21
 Chary R., Berger E., Cowie L., 2007, *ApJ*, **671**, 272
 Chiang J., Mukherjee R., 1998, *ApJ*, **496**, 752
 Cobb B. E., Bailyn C. D., van Dokkum P. G., Natarajan P., 2006, *ApJ*, **645**, L113
 Cucchiara A., et al., 2011, *ApJ*, **736**, 7
 Daigne F., Rossi E. M., Mochkovitch R., 2006, *MNRAS*, **372**, 1034
 Deng C.-M., Wang X.-G., Guo B.-B., Lu R.-J., Wang Y.-Z., Wei J.-J., Wu X.-F., Liang E.-W., 2016, *ApJ*, **820**, 66
 Dong X. F., Zhang Z. B., Zhang X. L., Li X. J., 2021, arXiv e-prints, [p. arXiv:2103.16347](https://arxiv.org/abs/2103.16347)
 Efron B., Petrosian V., 1992, *ApJ*, **399**, 345
 Fiore F., Guetta D., Piranomonte S., D'Elia V., Antonelli L. A., 2007, *A&A*, **470**, 515
 Firmani C., Avila-Reese V., Ghisellini G., Tutukov A. V., 2004, *ApJ*, **611**, 1033
 Foreman-Mackey D., Hogg D. W., Lang D., Goodman J., 2013, *PASP*, **125**, 306
 Frederiks D., et al., 2016a, GRB Coordinates Network, **20082**, 1
 Frederiks D., et al., 2016b, GRB Coordinates Network, **20323**, 1
 Frederiks D., et al., 2017, GRB Coordinates Network, **20604**, 1
 Frederiks D., et al., 2018a, GRB Coordinates Network, **22546**, 1
 Frederiks D., et al., 2018b, GRB Coordinates Network, **23424**, 1
 Gehrels N., et al., 2004, *ApJ*, **611**, 1005
 Golenetskii S., et al., 2015, GRB Coordinates Network, **18433**, 1
 Goodman J., Weare J., 2010, *Communications in Applied Mathematics and Computational Science*, **5**, 65
 Guetta D., Piran T., 2007, *J. Cosmology Astropart. Phys.*, **7**, 003
 Guetta D., Piran T., Waxman E., 2005, *ApJ*, **619**, 412
 Hamburg R., Veres P., Meegan C., Burns E., Connaughton V., Goldstein A., Kocevski D., Roberts O. J., 2019, GRB Coordinates Network, **23707**, 1
 Hjorth J., et al., 2003, *Nature*, **423**, 847
 Hopkins A. M., Beacom J. F., 2006, *ApJ*, **651**, 142

- Hui C. M., 2019, GRB Coordinates Network, **24002**, 1
- Jakobsson P., et al., 2006, *A&A*, **447**, 897
- Kaneko Y., Preece R. D., Briggs M. S., Paciesas W. S., Meegan C. A., Band D. L., 2006, *ApJS*, **166**, 298
- Kistler M. D., Yüksel H., Beacom J. F., Stanek K. Z., 2008, *ApJ*, **673**, L119
- Kistler M. D., Yüksel H., Beacom J. F., Hopkins A. M., Wyithe J. S. B., 2009, *ApJ*, **705**, L104
- Lan G.-X., Zeng H.-D., Wei J.-J., Wu X.-F., 2019, *MNRAS*, **488**, 4607
- Le T., Dermer C. D., 2007, *ApJ*, **661**, 394
- Le T., Ratke C., Mehta V., 2020, *MNRAS*, **493**, 1479
- Li L.-X., 2008, *MNRAS*, **388**, 1487
- Liang E., Zhang B., Virgili F., Dai Z. G., 2007, *ApJ*, **662**, 1111
- Liddle A. R., 2007, *MNRAS*, **377**, L74
- Lloyd-Ronning N. M., Fryer C. L., Ramirez-Ruiz E., 2002, *ApJ*, **574**, 554
- Lloyd-Ronning N. M., Aykutalp A., Johnson J. L., 2019, *MNRAS*, **488**, 5823
- Lu R.-J., Wei J.-J., Qin S.-F., Liang E.-W., 2012, *ApJ*, **745**, 168
- Lynden-Bell D., 1971, *MNRAS*, **155**, 95
- Mailyan B., 2018, GRB Coordinates Network, 22813, 1
- Mailyan B., Goldstein A., 2016, GRB Coordinates Network, **20192**, 1
- Markwardt C. B., et al., 2017, GRB Coordinates Network, **20456**, 1
- Marshall H. L., Tananbaum H., Avni Y., Zamorani G., 1983, *ApJ*, **269**, 35
- Narumoto T., Totani T., 2006, *ApJ*, **643**, 81
- Natarajan P., Albanna B., Hjorth J., Ramirez-Ruiz E., Tanvir N., Wijers R., 2005, *MNRAS*, **364**, L8
- Nava L., et al., 2012, *MNRAS*, **421**, 1256
- Paczynski B., 1998, *ApJ*, **494**, L45
- Palmer D. M., et al., 2018, GRB Coordinates Network, **22566**, 1
- Palmerio J. T., Daigne F., 2021, *A&A*, **649**, A166
- Paul D., 2018, *MNRAS*, **473**, 3385
- Pelassa V., 2014, GRB Coordinates Network, **16900**, 1
- Pescalli A., Ghirlanda G., Salafia O. S., Ghisellini G., Nappo F., Salvaterra R., 2015, *MNRAS*, **447**, 1911
- Pescalli A., et al., 2016, *A&A*, **587**, A40
- Petrosian V., Kitanidis E., Kocevski D., 2015, *ApJ*, **806**, 44
- Piran T., 2004, *Reviews of Modern Physics*, **76**, 1143
- Poolakkil S., Meegan C., Fermi GBM Team 2019a, GRB Coordinates Network, **24816**, 1
- Poolakkil S., Meegan C., Fermi GBM Team 2019b, GRB Coordinates Network, **25130**, 1
- Porciani C., Madau P., 2001, *ApJ*, **548**, 522
- Preece R. D., Briggs M. S., Mallozzi R. S., Pendleton G. N., Paciesas W. S., Band D. L., 2000, *ApJS*, **126**, 19
- Qin S.-F., Liang E.-W., Lu R.-J., Wei J.-Y., Zhang S.-N., 2010, *MNRAS*, **406**, 558
- Qu Y., Zeng H., Yan D., 2019, *MNRAS*, **490**, 758
- Robertson B. E., Ellis R. S., 2012, *ApJ*, **744**, 95
- Salvaterra R., Chincarini G., 2007, *ApJ*, **656**, L49
- Salvaterra R., Guidorzi C., Campana S., Chincarini G., Tagliaferri G., 2009a, *MNRAS*, **396**, 299
- Salvaterra R., et al., 2009b, *Nature*, **461**, 1258
- Salvaterra R., et al., 2012, *ApJ*, **749**, 68
- Soderberg A. M., et al., 2004, *Nature*, **430**, 648
- Stanbro M., Hui C. M., Meegan C., 2017, GRB Coordinates Network, **22277**, 1
- Stanek K. Z., et al., 2003, *ApJ*, **591**, L17
- Sun H., Zhang B., Li Z., 2015, *ApJ*, **812**, 33
- Svinkin D., et al., 2019, GRB Coordinates Network, **25974**, 1
- Tan W.-W., Wang F. Y., 2015, *MNRAS*, **454**, 1785
- Tan W.-W., Cao X.-F., Yu Y.-W., 2013, *ApJ*, **772**, L8
- Tanvir N. R., et al., 2009, *Nature*, **461**, 1254
- Totani T., 1997, *ApJ*, **486**, L71
- Tsvetkova A., et al., 2018a, GRB Coordinates Network, **22513**, 1
- Tsvetkova A., et al., 2018b, GRB Coordinates Network, **23363**, 1
- Tsvetkova A., et al., 2019a, GRB Coordinates Network, **23637**, 1
- Tsvetkova A., et al., 2019b, GRB Coordinates Network, **25660**, 1
- Veres P., Meegan C., Mailyan B., 2018, GRB Coordinates Network, 23053, 1
- Virgili F. J., Zhang B., Nagamine K., Choi J.-H., 2011, *MNRAS*, **417**, 3025
- Wanderman D., Piran T., 2010, *MNRAS*, **406**, 1944
- Wang F. Y., 2013, *A&A*, **556**, A90
- Wang F. Y., Dai Z. G., 2009, *MNRAS*, **400**, L10
- Wang F., Zou Y.-C., Liu F., Liao B., Liu Y., Chai Y., Xia L., 2020, *ApJ*, **893**, 77
- Wei J.-J., Wu X.-F., 2017, *International Journal of Modern Physics D*, **26**, 1730002
- Wei J.-J., Wu X.-F., Melia F., Wei D.-M., Feng L.-L., 2014, *MNRAS*, **439**, 3329
- Woosley S. E., 1993, in American Astronomical Society Meeting Abstracts #182. p. 894
- Woosley S. E., Bloom J. S., 2006, *ARA&A*, **44**, 507
- Yonetoku D., Murakami T., Nakamura T., Yamazaki R., Inoue A. K., Ioka K., 2004, *ApJ*, **609**, 935
- Yu H. F., 2014, GRB Coordinates Network, **17216**, 1
- Yu H., Wang F. Y., Dai Z. G., Cheng K. S., 2015, *ApJS*, **218**, 13
- Yüksel H., Kistler M. D., Beacom J. F., Hopkins A. M., 2008, *ApJ*, **683**, L5
- Zeng H., Yan D., Zhang L., 2014, *MNRAS*, **441**, 1760
- Zeng H., Melia F., Zhang L., 2016, *MNRAS*, **462**, 3094
- Zhang B., 2007, *Chinese J. Astron. Astrophys.*, **7**, 1
- Zhang B. B., 2014, GRB Coordinates Network, **16798**, 1
- Zhang B., Mészáros P., 2004, *International Journal of Modern Physics A*, **19**, 2385
- von Kienlin A., 2018a, GRB Coordinates Network, **22386**, 1
- von Kienlin A., 2018b, GRB Coordinates Network, **23320**, 1
- von Kienlin A., Burns E., 2015, GRB Coordinates Network, **17319**, 1

APPENDIX A: ADDITIONAL TABLE

Table A1: List of the bursts with known redshifts

GRB	Peak flux (photons cm ⁻² s ⁻¹)	z	α	β	E_p (keV)	$\log L$ (erg s ⁻¹)	Refs.
041228	1.61 ± 0.25	2.3	$-1.54^{+0.05}_{-0.05}$		$240.00^{+381.06}_{-66.53}$	52.09 ± 0.07	3, 3
050126	0.71 ± 0.17	1.29	$-1.10^{+0.10}_{-0.10}$	-2.20	$47.00^{+23.00}_{-8.00}$	51.02 ± 0.10	1, 3
050215B	0.67 ± 0.12	2.62	-1.10	$-2.20^{+0.60}_{-0.40}$	$17.60^{+6.10}_{-12.80}$	51.74 ± 0.08	1, 3
050219A	3.53 ± 0.35	0.211	$0.00^{+0.18}_{-0.18}$		$105.00^{+10.28}_{-6.65}$	49.74 ± 0.04	1, 3
050223	0.69 ± 0.16	0.5915	$-1.74^{+0.17}_{-0.18}$		$67.03^{+113.11}_{-22.99}$	50.15 ± 0.10	1, 4
050315	1.93 ± 0.22	1.949	-1.10	$-2.04^{+0.16}_{-0.24}$	$40.30^{+11.40}_{-11.40}$	51.96 ± 0.05	1, 3
050318	3.16 ± 0.20	1.44	$-1.22^{+0.45}_{-0.41}$		$50.86^{+12.24}_{-7.17}$	51.60 ± 0.03	1, 4
050319	1.52 ± 0.21	3.24	$-2.00^{+0.19}_{-0.21}$		$44.73^{+27.49}_{-43.11}$	52.54 ± 0.06	1, 4
050401	10.70 ± 0.92	2.9	$-1.44^{+0.08}_{-0.08}$		$165.49^{+391.26}_{-48.08}$	53.09 ± 0.04	1, 4
050406	0.36 ± 0.10	2.44	$-1.10^{+0.40}_{-0.40}$	$-2.56^{+0.35}_{-0.35}$	$25.00^{+35.00}_{-13.00}$	51.28 ± 0.12	2, 3
050410	1.80 ± 0.36	1.04	$-0.90^{+0.24}_{-0.24}$		$92.00^{+32.06}_{-13.31}$	51.06 ± 0.09	3, 3
050412	0.48 ± 0.05	4.5	$-0.60^{+0.12}_{-0.12}$		$640.00^{+574.62}_{-199.60}$	52.86 ± 0.05	3, 3
050416A	4.88 ± 0.48	0.6535	$-0.97^{+2.28}_{-1.01}$		$13.67^{+7.93}_{-12.56}$	51.00 ± 0.04	2, 3
050502B	1.42 ± 0.13	5.2	$-1.60^{+0.06}_{-0.06}$		$100.00^{+228.03}_{-19.96}$	52.78 ± 0.04	1, 3
050505	1.85 ± 0.31	4.27	$-1.41^{+0.12}_{-0.12}$		$140.25^{+343.09}_{-42.77}$	52.70 ± 0.07	1, 4
050525A	41.70 ± 0.94	0.606	$-1.10^{+0.03}_{-0.03}$		$84.10^{+1.03}_{-1.03}$	51.84 ± 0.01	2, 3
050603	21.50 ± 1.07	2.821	$-1.03^{+0.11}_{-0.11}$	$-2.03^{+0.17}_{-0.29}$	$343.70^{+87.00}_{-87.00}$	53.73 ± 0.02	3, 3
050607	0.95 ± 0.14	4	$-1.80^{+0.12}_{-0.12}$		$67.00^{+138.51}_{-16.94}$	52.39 ± 0.06	3, 3
050714B	0.52 ± 0.22	2.4383	$-0.42^{+1.93}_{-1.43}$		$28.71^{+7.26}_{-28.70}$	51.24 ± 0.18	1, 3
050716	2.18 ± 0.35	1.4	$-0.80^{+0.18}_{-0.18}$		$136.00^{+61.70}_{-18.15}$	51.57 ± 0.07	3, 3
050724	3.26 ± 0.30	0.257	$-1.66^{+0.17}_{-0.18}$		$100.00^{+376.82}_{-40.98}$	49.98 ± 0.04	2, 4
050730	0.55 ± 0.14	3.967	$-1.39^{+0.13}_{-0.13}$		$164.87^{+499.25}_{-59.36}$	52.12 ± 0.11	1, 4
050801	1.46 ± 0.14	1.38	$-1.90^{+0.12}_{-0.12}$		$44.00^{+35.08}_{-25.40}$	51.46 ± 0.04	1, 3
050802	2.75 ± 0.44	1.71	$-1.59^{+0.14}_{-0.15}$		$95.12^{+177.17}_{-31.15}$	51.88 ± 0.07	1, 4
050803	0.96 ± 0.11	3.5	$-1.30^{+0.06}_{-0.06}$		$235.00^{+382.27}_{-56.86}$	52.31 ± 0.05	1, 3
050814	0.71 ± 0.25	5.77	$-0.58^{+0.56}_{-0.56}$	-2.20	$54.00^{+7.50}_{-10.50}$	52.55 ± 0.15	1, 3
050819	0.38 ± 0.12	2.5043	$-0.65^{+2.62}_{-1.34}$		$20.19^{+16.66}_{-17.49}$	51.20 ± 0.14	1, 4
050820A	2.45 ± 0.23	2.612	$-1.20^{+0.06}_{-0.06}$		$490.00^{+435.50}_{-181.46}$	52.64 ± 0.04	2, 3
050822	2.24 ± 0.22	1.434	-1.00^*	$-2.21^{+0.14}_{-0.14}$	$27.25^{+7.09}_{-25.74}$	51.60 ± 0.04	1, 4
050824	0.50 ± 0.15	0.83	-1.00^*	$-2.91^{+0.43}_{-0.53}$	$13.85^{+2.74}_{-12.85}$	50.29 ± 0.13	1, 4
050826	0.38 ± 0.13	0.297	$-1.22^{+0.27}_{-0.27}$		$340.31^{+792.76}_{-209.24}$	49.42 ± 0.15	1, 4
050904	0.62 ± 0.17	6.29	$-1.17^{+0.07}_{-0.07}$		$531.78^{+775.65}_{-297.30}$	52.95 ± 0.12	1, 4
050908	0.70 ± 0.14	3.344	-1.10	-2.20	$41.00^{+9.00}_{-5.00}$	51.99 ± 0.09	1, 3
050911	1.33 ± 0.20	0.165	$-1.80^{+0.24}_{-0.24}$		$55.00^{+218.36}_{-31.45}$	49.15 ± 0.07	3, 3
050915A	0.77 ± 0.14	2.5273	$-1.30^{+0.12}_{-0.12}$		$179.00^{+321.18}_{-38.11}$	51.81 ± 0.08	2, 3
050922B	1.01 ± 0.36	4.5	-1.10	$-2.10^{+0.18}_{-0.18}$	$38.00^{+15.73}_{-22.38}$	52.49 ± 0.15	1, 3
050922C	7.26 ± 0.32	2.198	$-0.83^{+0.23}_{-0.26}$		$130.00^{+51.00}_{-27.00}$	52.56 ± 0.02	1, 3
051001	0.49 ± 0.11	2.4296	$-1.12^{+0.65}_{-0.56}$		$44.38^{+11.49}_{-8.01}$	51.32 ± 0.10	1, 4
051006	1.62 ± 0.30	1.059	$-1.40^{+0.12}_{-0.12}$		$270.00^{+350.82}_{-102.83}$	51.29 ± 0.08	1, 3
051008	5.44 ± 0.35	2.77	$-0.80^{+0.23}_{-0.22}$		$234.76^{+315.18}_{-70.12}$	52.89 ± 0.03	1, 4
051016B	1.30 ± 0.16	0.9364	-1.10	$-2.56^{+0.50}_{-6.33}$	$27.50^{+13.20}_{-12.30}$	50.81 ± 0.05	1, 3
051021B	0.80 ± 0.14	2.1	$-0.40^{+0.48}_{-0.48}$		$99.00^{+73.79}_{-19.36}$	51.47 ± 0.08	3, 3
051109A	3.94 ± 0.69	2.346	$-1.25^{+0.44}_{-0.59}$		$161.00^{+224.00}_{-58.00}$	52.42 ± 0.08	2, 3
051111	2.66 ± 0.21	1.55	$-1.22^{+0.09}_{-0.09}$	$-2.10^{+4.94}_{-0.27}$	$447.00^{+206.00}_{-175.00}$	52.19 ± 0.03	1, 3
051117B	0.49 ± 0.14	0.481	$-1.70^{+0.24}_{-0.24}$		$72.00^{+257.67}_{-22.38}$	49.78 ± 0.12	1, 3
051227	0.95 ± 0.12	0.8	$-1.10^{+0.12}_{-0.12}$		$340.00^{+387.11}_{-127.02}$	50.88 ± 0.05	3, 3
060108	0.77 ± 0.12	2	-1.10	$-2.01^{+0.01}_{-0.12}$	$44.00^{+16.94}_{-25.40}$	51.61 ± 0.07	1, 3
060110	1.89 ± 0.16	5	$-1.58^{+0.05}_{-0.05}$		$135.00^{+210.49}_{-28.43}$	52.89 ± 0.04	3, 3
060111A	1.71 ± 0.15	2.32	$-0.80^{+0.24}_{-0.24}$	$-2.29^{+0.15}_{-0.19}$	$83.00^{+14.52}_{-7.26}$	52.06 ± 0.04	1, 3
060111B	1.40 ± 0.27	1.5	$-0.90^{+0.12}_{-0.12}$	$-2.35^{+0.36}_{-4.63}$	$540.00^{+568.57}_{-169.36}$	52.05 ± 0.08	3, 3
060115	0.87 ± 0.12	3.53	$-1.15^{+0.58}_{-0.51}$		$69.81^{+121.75}_{-15.07}$	52.01 ± 0.06	1, 4
060123	0.04	0.56	$-1.90^{+0.60}_{-0.60}$		250.00*	49.03 ± 0.00	1, 3
060124	0.89 ± 0.18	2.296	$5.00^{+0.00}_{-2.89}$	$-2.00^{+0.00}_{-0.15}$	$29.64^{+3.67}_{-4.31}$	51.79 ± 0.09	1, 4
060202	0.51 ± 0.17	0.783	$-1.74^{+0.13}_{-0.13}$		$87.72^{+344.22}_{-26.36}$	50.34 ± 0.14	1, 4
060204B	1.35 ± 0.15	2.3393	$-0.70^{+0.18}_{-0.18}$		$125.00^{+47.18}_{-17.54}$	51.88 ± 0.05	1, 3
060206	2.79 ± 0.17	4.048	$-1.18^{+0.33}_{-0.31}$		$87.03^{+53.26}_{-15.82}$	52.70 ± 0.03	1, 4
060210	2.72 ± 0.28	3.91	$-1.47^{+0.10}_{-0.10}$		$136.23^{+347.11}_{-38.75}$	52.78 ± 0.04	1, 4

GRB	Peak flux (photons cm ⁻² s ⁻¹)	z	α	β	E_p (keV)	$\log L$ (erg s ⁻¹)	Refs.
060223A	1.35 ± 0.18	4.41	$-1.18^{+0.31}_{-0.31}$	-2.20	$71.00^{+100.00}_{-10.00}$	52.60 ± 0.06	2, 3
060306	5.97 ± 0.35	1.559	$-1.13^{+0.47}_{-0.43}$		$67.17^{+43.83}_{-11.66}$	51.98 ± 0.03	1, 4
060319	1.09 ± 0.14	1.172	-1.00^*	$-2.19^{+0.23}_{-0.26}$	$24.66^{+3.59}_{-23.66}$	51.09 ± 0.06	1, 4
060403	0.95 ± 0.13	1.3	$-0.40^{+0.24}_{-0.24}$		$247.00^{+239.53}_{-58.07}$	51.43 ± 0.06	3, 3
060418	6.52 ± 0.35	1.489	$-1.61^{+0.05}_{-0.05}$		$134.99^{+276.23}_{-33.35}$	52.16 ± 0.02	1, 4
060428B	0.66 ± 0.15	0.348	$-0.80^{+0.97}_{-0.97}$	$-2.20^{+0.40}_{-0.40}$	$23.00^{+3.00}_{-8.00}$	49.59 ± 0.10	3, 3
060501	1.98 ± 0.26	1.8	$-1.20^{+0.06}_{-0.06}$		$217.00^{+285.50}_{-52.62}$	51.91 ± 0.06	3, 3
060502A	1.69 ± 0.21	1.51	$-0.87^{+0.21}_{-0.15}$	$-1.98^{+0.16}_{-1.01}$	$174.00^{+87.10}_{-36.29}$	51.90 ± 0.05	3, 3
060505	2.65 ± 0.63	0.089				49.23 ± 0.10	1,
060510A	14.70 ± 1.13	1.2	$-1.80^{+0.06}_{-0.06}$		$74.00^{+146.98}_{-17.54}$	52.28 ± 0.03	3, 3
060510B	0.57 ± 0.11	4.94	$-1.47^{+0.18}_{-0.18}$	-2.20	$95.00^{+60.00}_{-30.00}$	52.38 ± 0.08	1, 3
060512	0.88 ± 0.20	2.1	$-0.50^{+3.80}_{-1.49}$		$22.31^{+11.50}_{-19.51}$	51.34 ± 0.10	1, 4
060522	0.55 ± 0.15	5.11	$-0.70^{+0.44}_{-0.44}$	-2.20	$70.00^{+13.00}_{-13.00}$	52.36 ± 0.12	1, 3
060526	1.67 ± 0.18	3.221	$-1.88^{+0.24}_{-0.25}$		$73.25^{+151.30}_{-72.25}$	52.45 ± 0.05	1, 4
060602A	0.56 ± 0.20	0.787	$-1.30^{+0.12}_{-0.12}$		$280.00^{+344.77}_{-90.73}$	50.53 ± 0.16	2, 3
060604	0.34 ± 0.13	2.1357	-1.00^*	$-2.17^{+0.54}_{-0.69}$	$36.82^{+49.21}_{-35.82}$	51.22 ± 0.17	1, 4
060605	0.46 ± 0.12	3.78	$-0.29^{+0.88}_{-0.73}$		$87.04^{+91.78}_{-19.90}$	51.80 ± 0.11	1, 4
060607A	1.40 ± 0.13	3.082	$-0.60^{+0.70}_{-0.60}$		$63.00^{+21.00}_{-10.00}$	52.00 ± 0.04	2, 3
060614	11.50 ± 0.74	0.125	$-1.90^{+0.04}_{-0.04}$		$393.02^{+818.57}_{-250.96}$	50.03 ± 0.03	1, 4
060707	1.01 ± 0.23	3.425	$-0.66^{+0.79}_{-0.67}$		$60.94^{+22.69}_{-9.27}$	51.97 ± 0.10	1, 4
060708	1.94 ± 0.14	1.92	$-1.00^{+0.30}_{-0.30}$		$99.00^{+73.79}_{-17.54}$	51.77 ± 0.03	1, 3
060714	1.28 ± 0.13	2.711	$-1.90^{+0.11}_{-0.11}$		$53.17^{+94.49}_{-49.44}$	52.16 ± 0.04	1, 4
060719	2.16 ± 0.20	1.532	$-1.93^{+0.11}_{-0.11}$		$54.88^{+44.95}_{-53.22}$	51.78 ± 0.04	1, 4
060729	1.17 ± 0.13	0.54	$-1.77^{+0.14}_{-0.14}$		$67.03^{+140.90}_{-28.43}$	50.30 ± 0.05	1, 4
060805A	0.34 ± 0.11	2.3633	$5.00^{+0.00}_{-4.46}$		$30.27^{+5.19}_{-4.39}$	50.85 ± 0.14	1, 4
060814	7.27 ± 0.29	1.9229	$-1.29^{+0.16}_{-0.15}$		$238.90^{+891.04}_{-83.43}$	52.56 ± 0.02	1, 4
060904B	2.44 ± 0.21	0.703	$-0.61^{+0.42}_{-0.42}$	$-1.78^{+0.23}_{-0.16}$	$103.00^{+59.00}_{-26.00}$	51.34 ± 0.04	1, 3
060906	1.97 ± 0.28	3.686	$-1.97^{+0.14}_{-0.14}$		$46.50^{+24.61}_{-44.93}$	52.73 ± 0.06	1, 4
060908	3.03 ± 0.25	1.8836	$-0.73^{+0.28}_{-0.26}$		$127.72^{+61.65}_{-24.75}$	52.01 ± 0.04	1, 4
060912A	8.58 ± 0.44	0.937	$-1.70^{+0.05}_{-0.05}$		$200.00^{+338.72}_{-66.53}$	51.84 ± 0.02	2, 3
060923B	1.52 ± 0.33	1.5094	-1.00^*	$-2.61^{+0.29}_{-0.33}$	$21.38^{+9.24}_{-19.33}$	51.38 ± 0.09	1, 4
060926	1.09 ± 0.14	3.2	-1.00^*	$-2.49^{+0.23}_{-0.25}$	$20.19^{+7.70}_{-18.73}$	52.06 ± 0.06	1, 4
060927	2.70 ± 0.17	5.47	$-0.82^{+0.43}_{-0.39}$		$70.90^{+21.82}_{-9.94}$	52.92 ± 0.03	1, 4
061004	2.54 ± 0.16	3.3	$-1.79^{+0.06}_{-0.06}$		$64.00^{+25.40}_{-13.31}$	52.60 ± 0.03	3, 3
061006A	5.24 ± 0.21	0.438	$-0.62^{+0.18}_{-0.21}$		$664.00^{+227.00}_{-144.00}$	51.47 ± 0.02	3, 3
061007	14.60 ± 0.37	1.261	$-0.96^{+0.03}_{-0.03}$		$838.02^{+1099.77}_{-326.78}$	52.95 ± 0.01	1, 4
061021	6.11 ± 0.27	0.3463	$-1.27^{+0.05}_{-0.05}$		$405.52^{+806.07}_{-167.84}$	50.82 ± 0.02	1, 4
061028	0.65 ± 0.19	0.76	$-1.70^{+0.18}_{-0.18}$		$79.00^{+262.51}_{-23.59}$	50.39 ± 0.13	3, 3
061110A	0.53 ± 0.12	0.758	$-1.60^{+0.06}_{-0.06}$		$106.00^{+181.46}_{-24.19}$	50.30 ± 0.10	2, 3
061110B	0.45 ± 0.11	3.44	$-0.70^{+0.12}_{-0.12}$	$-4.24^{+1.42}_{-3.48}$	$550.00^{+592.77}_{-151.22}$	52.45 ± 0.11	1, 3
061121	21.10 ± 0.46	1.314	$-1.31^{+0.02}_{-0.02}$	$-2.37^{+0.19}_{-0.73}$	$741.00^{+102.22}_{-381.06}$	52.95 ± 0.01	1, 3
061126	9.76 ± 0.38	1.1588	$-1.16^{+0.02}_{-0.02}$		$390.00^{+150.22}_{-150.00}$	52.31 ± 0.02	1, 3
061202	2.51 ± 0.17	2.2543	$-1.20^{+0.33}_{-0.31}$		$128.56^{+38.44}_{-38.44}$	52.13 ± 0.03	1, 4
061210	5.31 ± 0.47	0.41	$-0.76^{+0.15}_{-0.14}$		$544.04^{+763.39}_{-309.56}$	51.24 ± 0.04	2, 4
061222A	8.53 ± 0.26	2.088	$-0.94^{+0.08}_{-0.08}$	$-2.41^{+0.17}_{-0.73}$	$283.00^{+36.00}_{-25.00}$	52.93 ± 0.01	2, 3
061222B	1.59 ± 0.36	3.355	$-1.90^{+0.12}_{-0.12}$		$52.00^{+43.55}_{-26.01}$	52.48 ± 0.10	1, 3
070103	1.04 ± 0.15	2.6208	$-1.82^{+0.26}_{-0.28}$		$57.69^{+370.47}_{-43.13}$	51.98 ± 0.06	1, 4
070110	0.60 ± 0.12	2.352	$-1.15^{+0.44}_{-0.40}$		$108.33^{+4977.94}_{-33.17}$	51.51 ± 0.09	1, 4
070129	0.55 ± 0.12	2.3384	$-1.33^{+0.68}_{-0.59}$		$47.68^{+63.55}_{-12.48}$	51.38 ± 0.09	1, 4
070208	0.90 ± 0.22	1.165	$0.00^{+1.21}_{-0.60}$		$66.00^{+108.27}_{-19.96}$	50.76 ± 0.11	1, 3
070223	0.69 ± 0.15	1.6295	$-1.20^{+0.36}_{-0.36}$		$61.00^{+20.57}_{-9.07}$	51.09 ± 0.09	1, 3
070224	0.34 ± 0.11	1.9922	-1.00^*	$-2.27^{+0.28}_{-0.32}$	$29.58^{+12.80}_{-28.05}$	51.10 ± 0.14	1, 4
070306	4.07 ± 0.21	1.4959	$-1.67^{+0.10}_{-0.10}$		$119.60^{+335.79}_{-38.67}$	51.96 ± 0.02	1, 4
070318	1.76 ± 0.15	0.836	$-1.41^{+0.08}_{-0.08}$		$196.19^{+445.33}_{-78.00}$	51.00 ± 0.04	1, 4
070328	4.22 ± 0.24	2.0627	$-1.14^{+0.04}_{-0.04}$		$458.62^{+674.95}_{-180.14}$	52.63 ± 0.02	1, 4
070330	0.88 ± 0.14	2.4	$-0.33^{+1.07}_{-1.07}$	$-2.20^{+0.40}_{-0.40}$	$36.00^{+4.00}_{-4.00}$	51.72 ± 0.07	3, 3
070411	0.91 ± 0.13	2.954	$-1.70^{+0.10}_{-0.10}$		$119.81^{+555.97}_{-39.48}$	52.05 ± 0.06	1, 4
070419A	0.20 ± 0.10	0.97	$0.00^{+1.21}_{-1.21}$		$27.00^{+9.68}_{-11.49}$	49.80 ± 0.22	2, 3
070419B	1.38 ± 0.17	1.9591	$-1.36^{+0.19}_{-0.18}$		$172.74^{+730.74}_{-56.70}$	51.79 ± 0.05	1, 4

GRB	Peak flux (photons cm ⁻² s ⁻¹)	z	α	β	E_p (keV)	$\log L$ (erg s ⁻¹)	Refs.
070506	0.96 ± 0.13	2.31	5.00 ^{+0.00} _{-3.18}	-2.00 ^{+0.00} _{-0.37}	31.03 ^{+3.58} _{-4.56}	51.84 ± 0.06	1, 4
070508	24.10 ± 0.61	0.82	-0.81 ^{+0.04} _{-0.04}		188.00 ^{+4.84} _{-4.84}	52.15 ± 0.01	3, 3
070518	0.68 ± 0.13	1.161	-1.00*	-2.13 ^{+0.27} _{-0.29}	34.99 ^{+32.33} _{-33.43}	50.91 ± 0.08	1, 4
070521	6.53 ± 0.27	2.0865	-0.93 ^{+0.07} _{-0.07}		222.00 ^{+16.33} _{-12.70}	52.63 ± 0.02	1, 3
070529	1.43 ± 0.36	2.4996	-1.30 ^{+0.12} _{-0.12}		250.00 ^{+375.02} _{-78.63}	52.15 ± 0.11	1, 3
070611	0.82 ± 0.21	2.04	0.00 ^{+1.21} _{-0.60}		67.00 ^{+68.35} _{-15.73}	51.33 ± 0.11	1, 3
070612A	1.51 ± 0.38	0.617	-1.58 ^{+0.06} _{-0.06}		149.00 ^{+285.50} _{-35.69}	50.58 ± 0.11	2, 3
070621	2.50 ± 0.30	1.5	-1.55 ^{+0.04} _{-0.04}		157.00 ^{+230.45} _{-30.24}	51.76 ± 0.05	3, 3
070714A	2.70 ± 0.20	2.58	-2.56 ^{+0.21} _{-0.20}		250.00*	53.09 ± 0.03	3, 3
070714B	2.70 ± 0.20	0.92	-0.97 ^{+0.06} _{-0.06}	-2.12 ^{+0.42} _{-7.88}	543.75 ^{+355.73} _{-178.13}	51.84 ± 0.03	1, 3
070721B	1.50 ± 0.30	3.626	-1.20 ^{+0.06} _{-0.06}		410.00 ^{+489.94} _{-120.97}	52.71 ± 0.09	1, 3
070802	0.40 ± 0.10	2.45	-1.82 ^{+0.27} _{-0.29}		54.88 ^{+266.81} _{-35.43}	51.49 ± 0.11	1, 4
070808	2.00 ± 0.20	1.35	-1.50 ^{+0.12} _{-0.12}		135.00 ^{+270.37} _{-28.43}	51.52 ± 0.04	3, 3
070810A	1.90 ± 0.20	2.17	-0.70 ^{+0.48} _{-0.48}		41.00 ^{+4.84} _{-4.84}	51.72 ± 0.05	2, 3
071003	6.30 ± 0.40	1.6043	-0.97 ^{+0.07} _{-0.07}		799.00 ^{+124.00} _{-100.00}	52.82 ± 0.03	1, 3
071010A	0.80 ± 0.30	0.98	-1.00*	-2.11 ^{+0.39} _{-0.44}	36.79 ^{+49.23} _{-35.22}	50.81 ± 0.16	2, 4
071010B	7.70 ± 0.30	0.947	-1.25 ^{+0.45} _{-0.30}	-2.65 ^{+0.18} _{-0.30}	52.00 ^{+6.05} _{-8.47}	51.62 ± 0.02	1, 3
071011	1.70 ± 0.30	5	-1.40 ^{+0.06} _{-0.06}		370.00 ^{+465.74} _{-120.97}	53.01 ± 0.08	3, 3
071020	8.40 ± 0.30	2.145	-0.65 ^{+0.27} _{-0.32}		322.00 ^{+80.00} _{-53.00}	52.98 ± 0.02	1, 3
071021	0.70 ± 0.10	2.452	-1.73 ^{+0.22} _{-0.23}		74.08 ^{+424.00} _{-28.83}	51.70 ± 0.06	1, 4
071025	1.60 ± 0.20	5.2	-1.67 ^{+0.04} _{-0.04}		165.00 ^{+301.83} _{-35.69}	52.91 ± 0.05	1, 3
071028B	1.40 ± 0.50	0.94				51.28 ± 0.16	2, 3
071031	0.50 ± 0.10	2.692	-1.00*	-2.27 ^{+0.29} _{-0.32}	12.25 ^{+6.19} _{-11.25}	51.65 ± 0.09	1, 4
071101	0.40 ± 0.10	3.7	-1.10 ^{+0.40} _{-0.40}	-2.20 ^{+0.40} _{-0.40}	31.00 ^{+18.00} _{-18.00}	51.85 ± 0.11	3, 3
071112C	8.00 ± 1.00	0.823	-1.09 ^{+0.04} _{-0.04}		250.00*	51.73 ± 0.05	1, 3
071117	11.30 ± 0.40	1.331	-1.53 ^{+0.16} _{-0.15}		278.00 ^{+236.00} _{-79.00}	52.38 ± 0.02	1, 3
071122	0.40 ± 0.20	1.14	-1.60 ^{+0.24} _{-0.24}		111.00 ^{+317.55} _{-40.53}	50.63 ± 0.22	1, 3
080123	1.80 ± 0.40	0.495	-1.34 ^{+0.14} _{-0.14}		250.00*	50.52 ± 0.10	3, 3
080129	0.20 ± 0.10	4.349	-1.20 ^{+0.12} _{-0.12}		250.00 ^{+296.38} _{-90.73}	51.88 ± 0.22	1, 3
080205	1.40 ± 0.20	2.72	-2.00 ^{+0.06} _{-0.06}		50.00 ^{+21.17} _{-29.03}	52.32 ± 0.06	1, 3
080207	1.00 ± 0.30	2.0858	-1.05 ^{+0.41} _{-0.38}		102.50 ^{+127.50} _{-23.41}	51.58 ± 0.13	1, 4
080210	1.60 ± 0.20	2.641	-1.75 ^{+0.12} _{-0.12}		90.48 ^{+472.05} _{-36.46}	52.17 ± 0.05	1, 4
080310	1.30 ± 0.20	2.42	-1.00*	-2.35 ^{+0.17} _{-0.17}	22.31 ^{+8.32} _{-20.83}	51.87 ± 0.07	1, 4
080319A	1.20 ± 0.20	2.0265	-1.60 ^{+0.06} _{-0.06}		105.00 ^{+181.46} _{-21.17}	51.72 ± 0.07	1, 3
080319B	24.80 ± 0.50	0.937	-0.82 ^{+0.01} _{-0.01}	-3.87 ^{+0.44} _{-1.09}	651.00 ^{+13.00} _{-14.00}	52.84 ± 0.01	1, 3
080319C	5.20 ± 0.30	1.95	-1.00 ^{+0.18} _{-0.18}		157.00 ^{+183.27} _{-30.24}	52.34 ± 0.03	1, 3
080320	0.60 ± 0.10	7	-1.60 ^{+0.18} _{-0.18}		95.00 ^{+293.36} _{-23.59}	52.70 ± 0.07	3, 3
080325	1.40 ± 0.60	1.78	-1.67 ^{+0.17} _{-0.18}		110.52 ^{+398.86} _{-41.46}	51.67 ± 0.19	1, 4
080330	0.90 ± 0.20	1.51	-1.00*	-2.38 ^{+0.41} _{-0.48}	20.19 ^{+6.58} _{-19.19}	51.21 ± 0.10	1, 4
080411	43.20 ± 0.90	1.03	-1.68 ^{+0.03} _{-0.03}		405.52 ^{+806.07} _{-223.53}	52.74 ± 0.01	1, 4
080413A	5.60 ± 0.20	2.433	-1.56 ^{+0.04} _{-0.04}		149.00 ^{+25.40} _{-25.40}	52.62 ± 0.02	2, 3
080413B	18.70 ± 0.80	1.1	-1.26 ^{+0.16} _{-0.16}		73.30 ^{+9.56} _{-9.56}	52.13 ± 0.02	1, 3
080430	2.60 ± 0.20	0.767	-1.74 ^{+0.09} _{-0.09}		122.14 ^{+533.65} _{-46.59}	51.06 ± 0.03	1, 4
080515	3.90 ± 0.70	2.47	0.00 ^{+0.60} _{-0.60}		26.00 ^{+3.02} _{-3.02}	52.10 ± 0.08	1, 3
080516	1.80 ± 0.30	3.2	-1.80 ^{+0.18} _{-0.18}		67.00 ^{+243.16} _{-22.98}	52.43 ± 0.07	2, 3
080520	0.50 ± 0.10	1.545	-1.00*	-3.35 ^{+0.63} _{-0.88}	11.08 ^{+3.06} _{-10.08}	51.02 ± 0.09	1, 4
080602	2.90 ± 0.20	1.8204	-1.51 ^{+0.13} _{-0.14}		116.18 ^{+251.68} _{-43.94}	51.98 ± 0.03	1, 4
080603B	3.50 ± 0.20	2.69	-1.23 ^{+0.45} _{-0.33}		102.00 ^{+71.98} _{-16.94}	52.41 ± 0.02	1, 3
080604	0.40 ± 0.10	1.416	-1.70 ^{+0.12} _{-0.12}		74.00 ^{+256.46} _{-17.54}	50.85 ± 0.11	1, 3
080605	19.90 ± 0.60	1.6398	-1.13 ^{+0.15} _{-0.15}		227.84 ^{+249.64} _{-64.41}	52.84 ± 0.01	1, 4
080607	23.10 ± 1.10	3.036	-1.17 ^{+0.04} _{-0.04}		902.50 ^{+1169.78} _{-469.32}	53.95 ± 0.02	1, 4
080707	1.00 ± 0.10	1.23	-1.71 ^{+0.19} _{-0.19}		74.08 ^{+317.31} _{-31.97}	51.10 ± 0.04	1, 4
080710	1.00 ± 0.20	0.845	-1.30 ^{+0.12} _{-0.12}		300.00 ^{+332.67} _{-120.97}	50.88 ± 0.09	1, 3
080721	20.90 ± 1.80	2.591	-0.95 ^{+0.09} _{-0.09}		604.96 ^{+979.46} _{-292.44}	53.74 ± 0.04	1, 4
080804	3.10 ± 0.40	2.2045	-1.03 ^{+0.11} _{-0.11}		405.52 ^{+650.03} _{-204.15}	52.56 ± 0.06	1, 4
080805	1.10 ± 0.10	1.505	-1.54 ^{+0.09} _{-0.09}		300.42 ^{+552.02} _{-188.93}	51.51 ± 0.04	1, 4
080810	2.00 ± 0.20	3.35	-1.31 ^{+0.12} _{-0.12}		366.93 ^{+616.00} _{-217.69}	52.69 ± 0.04	1, 4
080905B	0.50 ± 0.10	2.374	-0.85 ^{+0.14} _{-0.14}	-2.28 ^{+0.38} _{-0.38}	179.00 ^{+36.29} _{-36.29}	51.74 ± 0.09	1, 3
080906	1.00 ± 0.20	2.1	-1.58 ^{+0.05} _{-0.05}		105.00 ^{+142.75} _{-18.75}	51.67 ± 0.09	1, 3

GRB	Peak flux (photons cm ⁻² s ⁻¹)	z	α	β	E_p (keV)	$\log L$ (erg s ⁻¹)	Refs.
080913	1.40 ± 0.20	6.695	$-0.40^{+0.88}_{-0.74}$		$98.20^{+135.40}_{-22.89}$	52.91 ± 0.06	1, 4
080916A	2.70 ± 0.20	0.689	$-1.00^{+0.23}_{-0.19}$		$129.00^{+19.96}_{-12.70}$	50.88 ± 0.03	2, 3
080916B	0.60 ± 0.20	4.35	$-1.50^{+0.12}_{-0.12}$		$100.00^{+228.03}_{-22.38}$	52.19 ± 0.14	3, 3
080928	2.10 ± 0.10	1.692	$-1.70^{+0.06}_{-0.06}$		$74.00^{+146.98}_{-15.73}$	51.77 ± 0.02	1, 3
081007	2.60 ± 0.40	0.5295	$-1.35^{+1.02}_{-0.64}$		$27.25^{+11.37}_{-15.73}$	50.45 ± 0.07	1, 4
081008	1.30 ± 0.10	1.9685	$-1.30^{+0.34}_{-0.31}$		$105.25^{+426.59}_{-29.00}$	51.66 ± 0.03	1, 4
081028A	0.50 ± 0.10	3.038	$-1.30^{+0.24}_{-0.24}$		$67.00^{+18.75}_{-7.86}$	51.64 ± 0.09	2, 3
081029	0.50 ± 0.20	3.8479	$-1.40^{+0.12}_{-0.12}$		$300.00^{+332.67}_{-120.97}$	52.17 ± 0.17	1, 3
081102A	1.40 ± 0.30	3.04	$-0.84^{+0.15}_{-0.17}$		$80.00^{+9.68}_{-6.05}$	52.06 ± 0.09	3, 3
081109A	1.10 ± 0.00	0.9787	$-0.67^{+1.85}_{-1.85}$	$-1.65^{+0.03}_{-0.03}$	$32.40^{+38.30}_{-38.30}$	51.34 ± 0.00	1, 3
081118	0.60 ± 0.20	2.58	-1.00^*	$-2.14^{+0.18}_{-0.19}$	$36.79^{+12.18}_{-35.22}$	51.68 ± 0.14	1, 4
081121	4.40 ± 1.00	2.512	$-0.52^{+0.56}_{-0.50}$		$133.77^{+163.06}_{-33.28}$	52.50 ± 0.10	1, 4
081203A	2.90 ± 0.20	2.1	$-1.44^{+0.04}_{-0.04}$		$201.00^{+266.14}_{-45.36}$	52.22 ± 0.03	2, 3
081210	2.50 ± 0.20	2.0631	$-1.40^{+0.06}_{-0.06}$		$220.00^{+356.87}_{-66.53}$	52.15 ± 0.03	1, 3
081221	18.20 ± 0.50	2.26	$-1.10^{+0.15}_{-0.14}$	$-29.44^{+27.20}_{-85.56}$	$82.60^{+7.67}_{-5.40}$	52.89 ± 0.01	1, 4
081222	7.70 ± 0.20	2.77	$-1.04^{+0.17}_{-0.17}$		$136.22^{+53.27}_{-24.01}$	52.84 ± 0.01	1, 4
081228	0.60 ± 0.10	3.44	$-2.00^{+0.18}_{-0.18}$		$39.00^{+47.18}_{-20.57}$	52.20 ± 0.07	1, 3
081230	0.70 ± 0.10	2	$-1.00^{+0.48}_{-0.48}$		$52.00^{+11.49}_{-8.47}$	51.26 ± 0.06	1, 3
090102	5.50 ± 0.80	1.547	$-1.36^{+0.10}_{-0.10}$		$366.93^{+616.00}_{-217.69}$	52.31 ± 0.06	1, 4
090113	2.50 ± 0.20	1.7493	$-1.52^{+0.10}_{-0.10}$		$128.40^{+434.15}_{-39.65}$	51.89 ± 0.03	1, 4
090201	14.70 ± 1.00	2.1	$-0.97^{+0.05}_{-0.05}$	$-2.80^{+0.31}_{-0.31}$	254.84	53.08 ± 0.03	1, 3
090205	0.50 ± 0.10	4.6497	$-0.89^{+1.69}_{-1.10}$		$33.29^{+31.16}_{-28.99}$	51.95 ± 0.09	1, 4
090313	0.80 ± 0.30	3.375	$-1.89^{+0.29}_{-0.32}$		$54.88^{+202.37}_{-51.09}$	52.18 ± 0.16	1, 4
090401B	23.10 ± 0.50	3.1	$-0.89^{+0.11}_{-0.11}$	$-2.32^{+0.21}_{-0.39}$	$205.00^{+55.00}_{-37.00}$	53.69 ± 0.01	3, 3
090404	1.90 ± 0.20	3	$-1.80^{+0.24}_{-0.12}$		$31.00^{+2.42}_{-18.15}$	52.35 ± 0.05	1, 3
090407	0.60 ± 0.10	1.4485	$-1.48^{+0.37}_{-0.38}$		$100.00^{+497.93}_{-49.96}$	51.02 ± 0.07	1, 4
090417B	0.30 ± 0.10	0.345	$-1.70^{+0.06}_{-0.06}$		$111.00^{+428.24}_{-24.80}$	49.26 ± 0.14	1, 3
090418A	1.90 ± 0.30	1.608	$-1.30^{+0.09}_{-0.09}$		$610.00^{+554.00}_{-215.00}$	52.04 ± 0.07	2, 3
090423	1.70 ± 0.20	8.26	$-0.70^{+0.62}_{-0.55}$		$50.55^{+9.35}_{-5.66}$	53.07 ± 0.05	1, 4
090424	71.00 ± 2.00	0.544	$-1.08^{+0.16}_{-0.15}$		$126.08^{+37.02}_{-18.86}$	52.05 ± 0.01	1, 4
090429B	1.60 ± 0.20	9.2	$-0.47^{+0.47}_{-0.47}$		$42.10^{+3.39}_{-3.39}$	53.10 ± 0.05	1, 3
090516A	1.60 ± 0.20	4.109	$-1.52^{+0.03}_{-0.03}$	$-2.30^{+0.16}_{-0.16}$	$142.00^{+15.73}_{-15.73}$	52.67 ± 0.05	2, 3
090519	0.60 ± 0.20	3.85	$-0.98^{+0.22}_{-0.21}$		$405.52^{+806.07}_{-223.52}$	52.44 ± 0.14	1, 4
090529	0.40 ± 0.10	2.625	$-1.00^{+0.60}_{-0.60}$		$43.00^{+18.75}_{-10.28}$	51.29 ± 0.11	1, 3
090530	2.50 ± 0.30	1.266	$-1.60^{+0.12}_{-0.12}$		$90.00^{+130.05}_{-19.96}$	51.51 ± 0.05	1, 3
090618	38.90 ± 0.80	0.54	$-1.26^{+0.04}_{-0.01}$	$-2.50^{+0.09}_{-0.20}$	$155.50^{+6.71}_{-6.35}$	51.93 ± 0.01	1, 3
090709A	7.80 ± 0.30	1.8	$-0.85^{+0.05}_{-0.05}$	$-2.70^{+0.15}_{-0.15}$	478.93	52.93 ± 0.02	3, 3
090715B	3.80 ± 0.20	3	$-1.10^{+0.40}_{-0.34}$		$134.00^{+56.00}_{-30.00}$	52.61 ± 0.02	1, 3
090726	0.70 ± 0.20	2.71	$-1.20^{+0.79}_{-0.48}$		$27.00^{+7.86}_{-13.31}$	51.60 ± 0.12	1, 3
090809	1.10 ± 0.20	2.737	$-1.70^{+0.51}_{-0.57}$		$74.08^{+825.80}_{-68.05}$	52.00 ± 0.08	1, 4
090812	3.60 ± 0.20	2.452	$-1.29^{+0.06}_{-0.06}$		$271.83^{+522.06}_{-117.45}$	52.55 ± 0.02	1, 4
090814A	0.60 ± 0.20	0.7	$-1.84^{+0.19}_{-0.18}$		250.00^*	50.43 ± 0.14	3, 3
090904B	1.90 ± 0.20	5	$-1.13^{+0.04}_{-0.04}$	$-2.30^{+0.07}_{-0.07}$	$113.00^{+6.65}_{-6.65}$	52.91 ± 0.05	3, 3
090926B	3.20 ± 0.30	1.24	$-0.13^{+0.04}_{-0.04}$		$91.00^{+1.21}_{-1.21}$	51.48 ± 0.04	1, 3
090927	2.00 ± 0.20	1.37	$-1.77^{+0.34}_{-0.37}$		$60.65^{+527.35}_{-55.11}$	51.53 ± 0.04	1, 4
091018	10.30 ± 0.40	0.971	$-1.69^{+0.32}_{-0.30}$		$22.74^{+8.45}_{-21.57}$	51.80 ± 0.02	1, 4
091020	4.20 ± 0.30	1.71	$-1.24^{+0.31}_{-0.29}$		$140.04^{+1827.70}_{-45.38}$	52.08 ± 0.03	1, 4
091024	2.00 ± 0.30	1.092	$-1.28^{+0.07}_{-0.07}$		$349.03^{+599.50}_{-172.23}$	51.50 ± 0.07	1, 4
091029	1.80 ± 0.10	2.752	$-1.40^{+0.32}_{-0.30}$		$59.35^{+19.53}_{-8.01}$	52.10 ± 0.02	1, 4
091109A	1.30 ± 0.40	3.076	$-1.23^{+0.27}_{-0.26}$		$448.17^{+847.42}_{-272.07}$	52.49 ± 0.13	2, 4
091127	46.50 ± 2.70	0.49	-1.00^*	$-2.13^{+0.08}_{-0.09}$	$27.25^{+5.23}_{-26.25}$	51.83 ± 0.03	1, 4
091208B	15.20 ± 1.00	1.063	$-1.29^{+0.08}_{-0.07}$	$-2.28^{+0.07}_{-0.08}$	$108.63^{+73.34}_{-57.60}$	52.22 ± 0.03	1, 3
100219A	0.40 ± 0.10	4.6667	$-1.37^{+0.26}_{-0.26}$		$122.14^{+422.09}_{-51.71}$	52.09 ± 0.11	1, 4
100302A	0.50 ± 0.10	4.813	-1.00^*	$-2.03^{+0.23}_{-0.24}$	$42.74^{+31.28}_{-41.13}$	52.27 ± 0.09	1, 4
100316A	2.30 ± 0.40	3.155	$-1.54^{+0.23}_{-0.23}$		$128.40^{+434.15}_{-60.53}$	52.48 ± 0.08	1, 4
100316B	1.30 ± 0.10	1.18	-1.00^*	$-2.29^{+0.22}_{-0.24}$	$28.65^{+13.90}_{-27.13}$	51.13 ± 0.03	1, 4
100316D	0.10 ± 0.00	0.059	$-2.29^{+0.41}_{-0.41}$		250.00^*	49.39 ± 0.00	3, 3
100413A	0.70 ± 0.10	3.9	$-1.22^{+0.03}_{-0.03}$	-2.20	$959.00^{+200.21}_{-200.21}$	52.66 ± 0.06	2, 3
100418A	1.00 ± 0.20	0.6235	-1.00^*	$-2.06^{+0.27}_{-0.29}$	$36.79^{+16.80}_{-35.79}$	50.47 ± 0.09	1, 4

GRB	Peak flux (photons cm ⁻² s ⁻¹)	<i>z</i>	α	β	E_p (keV)	$\log L$ (erg s ⁻¹)	Refs.
100424A	0.40 ± 0.10	2.465	$-1.87^{+0.14}_{-0.14}$		54.88 $^{+98.76}_{-32.70}$	51.52 ± 0.11	1, 4
100425A	1.40 ± 0.20	1.755	$-0.53^{+2.83}_{-1.46}$		23.46 $^{+11.94}_{-21.36}$	51.35 ± 0.06	1, 4
100508A	0.40 ± 0.20	0.5201	$-1.23^{+0.25}_{-0.25}$		201.38 $^{+557.34}_{-101.31}$	49.87 ± 0.22	1, 4
100513A	0.60 ± 0.10	4.772	$-1.65^{+0.14}_{-0.14}$		81.87 $^{+258.16}_{-23.28}$	52.31 ± 0.07	1, 4
100606A	1.60 ± 0.40	1.5545	$-1.05^{+0.14}_{-0.14}$		945.00 $^{+551.00}_{-266.00}$	52.20 ± 0.11	3, 3
100615A	5.40 ± 0.20	1.398	$-0.90^{+0.18}_{-0.18}$	$-1.80^{+0.03}_{-0.03}$	53.30 $^{+9.90}_{-9.90}$	52.26 ± 0.02	1, 3
100621A	12.80 ± 0.30	0.542	$-1.70^{+0.08}_{-0.08}$	$-2.45^{+1.44}_{-1.44}$	95.00 $^{+8.00}_{-11.00}$	51.41 ± 0.01	1, 3
100704A	4.30 ± 0.20	3.6	$-0.93^{+0.05}_{-0.05}$	$-2.00^{+0.08}_{-0.08}$	175.00 $^{+18.15}_{-18.15}$	53.14 ± 0.02	2, 3
100724A	1.90 ± 0.20	1.288	$-0.76^{+0.01}_{-0.01}$	$-2.03^{+0.02}_{-0.02}$	413.10 $^{+8.90}_{-8.90}$	52.07 ± 0.05	3, 3
100728A	5.10 ± 0.20	1.567	$-0.75^{+0.01}_{-0.01}$	$-3.04^{+0.34}_{-0.34}$	344.00 $^{+5.44}_{-5.44}$	52.48 ± 0.02	1, 3
100728B	3.50 ± 0.50	2.106	$-0.80^{+0.12}_{-0.12}$	$-2.20^{+0.12}_{-0.12}$	104.00 $^{+8.47}_{-8.47}$	52.35 ± 0.06	1, 3
100805A	0.70 ± 0.20	1.3	-1.00*		64.00	50.83 ± 0.12	2, 3
100814A	2.50 ± 0.20	1.44	$-0.64^{+0.08}_{-0.08}$	$-2.02^{+0.07}_{-0.07}$	106.00 $^{+8.47}_{-8.47}$	51.92 ± 0.03	1, 3
100816A	10.90 ± 0.40	0.8034	$-1.00^{+0.24}_{-0.18}$		148.00 $^{+24.80}_{-15.73}$	51.69 ± 0.02	2, 3
100901A	0.80 ± 0.20	1.408	$-1.55^{+0.22}_{-0.23}$		128.40 $^{+568.43}_{-54.79}$	51.16 ± 0.11	1, 4
100902A	1.00 ± 0.10	4.5	$-1.96^{+0.14}_{-0.14}$		49.66 $^{+50.27}_{-48.02}$	52.64 ± 0.04	2, 4
100905A	0.60 ± 0.10	7.9	$-1.27^{+0.22}_{-0.21}$		164.87 $^{+499.25}_{-73.13}$	52.85 ± 0.07	1, 4
100906A	10.10 ± 0.40	1.727	$-1.34^{+0.05}_{-0.05}$	$-1.98^{+0.04}_{-0.04}$	106.00 $^{+10.89}_{-10.89}$	52.66 ± 0.02	1, 3
101213A	2.20 ± 0.40	0.414	$-1.37^{+0.09}_{-0.09}$		405.52 $^{+650.03}_{-243.39}$	50.53 ± 0.08	1, 4
101219B	0.60 ± 0.30	0.55	$-1.37^{+0.72}_{-0.72}$	$-2.26^{+0.14}_{-0.14}$	56.40 $^{+6.60}_{-6.60}$	50.06 ± 0.22	1, 3
110106B	2.10 ± 0.30	0.618	$-1.40^{+0.25}_{-0.12}$		111.00 $^{+35.69}_{-15.73}$	50.65 ± 0.06	1, 3
110128A	0.80 ± 0.20	2.339	$-1.26^{+0.25}_{-0.25}$		192.00 $^{+112.00}_{-112.00}$	51.76 ± 0.11	1, 3
110205A	3.60 ± 0.20	2.22	$-1.52^{+0.09}_{-0.09}$	$-2.36^{+0.31}_{-0.31}$	222.00 $^{+46.00}_{-46.00}$	52.44 ± 0.02	1, 3
110213A	1.60 ± 0.60	1.46	$-1.44^{+0.03}_{-0.03}$	$-2.36^{+0.31}_{-0.31}$	98.00 $^{+4.00}_{-5.00}$	51.55 ± 0.16	1, 3
110422A	30.70 ± 1.00	1.77	$-0.65^{+0.04}_{-0.04}$	$-2.96^{+0.08}_{-0.11}$	152.00 $^{+3.02}_{-3.02}$	53.08 ± 0.01	1, 3
110503A	1.35 ± 0.06	1.613	$-0.88^{+0.15}_{-0.15}$		133.00 $^{+32.66}_{-32.66}$	51.50 ± 0.02	1, 3
110709B	3.40 ± 0.30	2.09	$-1.00^{+0.14}_{-0.13}$		278.00 $^{+43.00}_{-32.00}$	52.41 ± 0.04	1, 3
110715A	53.90 ± 1.10	0.82	$-1.23^{+0.05}_{-0.05}$	$-2.70^{+0.12}_{-0.30}$	120.00 $^{+7.26}_{-6.65}$	52.43 ± 0.01	1, 3
110726A	1.00 ± 0.20	1.04	$-0.64^{+0.53}_{-0.53}$		46.50 $^{+7.14}_{-7.14}$	50.66 ± 0.09	3, 3
110731A	11.00 ± 0.30	2.83	$-0.82^{+0.03}_{-0.03}$	$-2.32^{+0.02}_{-0.03}$	311.52 $^{+35.46}_{-31.52}$	53.43 ± 0.01	1, 3
110801A	1.10 ± 0.20	1.858	$-1.70^{+0.22}_{-0.15}$		140.00 $^{+1270.00}_{-59.90}$	51.65 ± 0.08	1, 3
110808A	0.40 ± 0.20	1.348	$-1.13^{+0.08}_{-0.08}$		2960.00 $^{+1217.00}_{-796.00}$	51.70 ± 0.22	1, 3
110818A	1.60 ± 0.30	3.36	$-1.11^{+0.17}_{-0.17}$	$-1.76^{+0.10}_{-0.10}$	183.00 $^{+85.00}_{-85.00}$	52.71 ± 0.08	1, 3
111008A	6.40 ± 0.70	4.9898	$-1.36^{+0.24}_{-0.21}$		149.00 $^{+52.00}_{-28.00}$	53.40 ± 0.05	1, 3
111107A	1.20 ± 0.20	2.893	$-1.38^{+0.21}_{-0.21}$		27.74 $^{+8.22}_{-8.22}$	51.95 ± 0.07	1, 3
111123A	0.90 ± 0.10	3.1516	$-1.30^{+0.26}_{-0.24}$		25.96 $^{+30.20}_{-6.03}$	51.90 ± 0.05	1, 3
111129A	0.90 ± 0.20	1.0796	-1.00*	$-2.65^{+0.44}_{-0.55}$	16.53 $^{+4.83}_{-15.53}$	50.82 ± 0.10	1, 4
111209A	0.50 ± 0.10	0.677	$-1.31^{+0.09}_{-0.09}$		310.00 $^{+53.00}_{-53.00}$	50.35 ± 0.09	2, 3
111212A	0.80 ± 0.30	0.269				49.75 ± 0.16	2,
111215A	0.50 ± 0.20	2.06	$-1.41^{+0.35}_{-0.36}$		122.14 $^{+553.65}_{-57.14}$	51.34 ± 0.17	1, 4
111225A	0.70 ± 0.10	0.297	$-1.67^{+0.16}_{-0.16}$		77.88 $^{+250.45}_{-27.47}$	49.43 ± 0.06	1, 4
111228A	12.40 ± 0.50	0.714	$-1.90^{+0.06}_{-0.06}$	$-2.70^{+0.18}_{-0.18}$	34.00 $^{+1.81}_{-1.81}$	51.68 ± 0.02	1, 3
111229A	1.00 ± 0.20	1.3805	-1.00*	$-2.01^{+0.31}_{-0.35}$	44.93 $^{+56.78}_{-43.31}$	51.34 ± 0.09	1, 4
120118B	2.20 ± 0.30	2.943	$-0.30^{+0.29}_{-0.29}$	$-2.55^{+0.15}_{-0.15}$	43.10 $^{+3.90}_{-3.90}$	52.22 ± 0.06	1, 3
120119A	10.30 ± 0.30	1.728	$-0.96^{+0.03}_{-0.03}$	$-2.37^{+0.09}_{-0.09}$	183.00 $^{+7.00}_{-7.00}$	52.69 ± 0.01	1, 3
120211A	0.50 ± 0.20	2.4	$-1.44^{+0.26}_{-0.27}$		116.18 $^{+410.33}_{-53.94}$	51.50 ± 0.17	1, 4
120224A	0.90 ± 0.20	1.1	-1.00*	$-2.22^{+0.44}_{-0.54}$	33.29 $^{+21.80}_{-32.29}$	50.92 ± 0.10	1, 4
120326A	4.60 ± 0.20	1.798	$-0.98^{+0.08}_{-0.08}$	$-2.53^{+0.09}_{-0.09}$	46.50 $^{+2.24}_{-2.24}$	52.07 ± 0.02	1, 3
120327A	3.90 ± 0.20	2.813	$-1.14^{+0.26}_{-0.28}$		27.82 $^{+5.97}_{-21.01}$	52.37 ± 0.02	1, 3
120404A	1.20 ± 0.20	2.876	$-1.84^{+0.14}_{-0.14}$		60.65 $^{+167.03}_{-25.27}$	52.15 ± 0.07	1, 4
120422A	0.60 ± 0.20	0.283	$-1.90^{+0.44}_{-0.49}$		40.66 $^{+306.42}_{-38.26}$	49.38 ± 0.14	1, 4
120521C	1.90 ± 0.20	6	$-1.68^{+0.12}_{-0.12}$		77.88 $^{+195.76}_{-24.59}$	53.05 ± 0.05	1, 4
120712A	2.40 ± 0.20	4.1745	$-0.60^{+0.20}_{-0.20}$	$-1.80^{+0.20}_{-0.20}$	23.96 $^{+5.02}_{-5.02}$	52.94 ± 0.04	1, 3
120714B	0.40 ± 0.10	0.3984	$-0.29^{+0.96}_{-0.80}$		43.48 $^{+7.31}_{-18.54}$	49.21 ± 0.11	1, 3
120722A	1.00 ± 0.30	0.9586	$-1.95^{+0.26}_{-0.28}$		49.66 $^{+50.27}_{-48.66}$	50.95 ± 0.13	1, 4
120724A	0.60 ± 0.20	1.48	$-0.53^{+0.93}_{-0.93}$		27.60 $^{+4.54}_{-4.54}$	50.78 ± 0.14	1, 3
120729A	2.90 ± 0.20	0.8	$-1.62^{+0.08}_{-0.08}$		106.67	51.11 ± 0.03	1, 3
120802A	3.00 ± 0.20	3.796	$-1.21^{+0.28}_{-0.28}$		57.20 $^{+11.73}_{-11.73}$	52.61 ± 0.03	1, 3
120805A	0.37 ± 0.20	3.1	$-0.08^{+1.77}_{-1.27}$		84.33 $^{+764.14}_{-21.60}$	51.49 ± 0.23	1, 4

GRB	Peak flux (photons cm ⁻² s ⁻¹)	z	α	β	E_p (keV)	$\log L$ (erg s ⁻¹)	Refs.
120811C	4.10 ± 0.20	2.671	-1.40 ^{+0.18} _{-0.18}		42.90 ^{+3.45} _{-3.45}	52.41 ± 0.02	1, 3
120815A	2.20 ± 0.30	2.358	-1.00*	-2.47 ^{+0.26} _{-0.30}	23.46 ^{+10.13} _{-21.36}	52.04 ± 0.06	1, 4
120907A	2.90 ± 0.40	0.97	-0.75 ^{+0.25} _{-0.25}		154.52 ^{+32.89} _{-32.89}	51.35 ± 0.06	1, 3
120909A	1.80 ± 0.30	3.93	-0.83 ^{+0.08} _{-0.08}	-1.92 ^{+0.09} _{-0.09}	195.00 ^{+25.00} _{-25.00}	52.92 ± 0.07	2, 3
120922A	2.00 ± 0.20	3.1	-1.60 ^{+0.42} _{-0.42}	-2.30 ^{+0.06} _{-0.06}	37.70 ^{+2.12} _{-2.12}	52.41 ± 0.04	1, 3
120923A	0.60 ± 0.10	7.8	-0.29 ^{+1.00} _{-1.00}		44.40 ^{+6.41} _{-6.41}	52.51 ± 0.07	1, 3
121024A	1.30 ± 0.20	2.298	-1.36 ^{+0.16} _{-0.16}		245.96 ^{+621.09} _{-127.14}	52.01 ± 0.07	1, 4
121027A	1.30 ± 0.20	1.773	-1.49 ^{+0.43} _{-0.39}		61.75 ^{+437.65} _{-13.25}	51.52 ± 0.07	1, 4
121117A	1.10 ± 0.10	3.1	-1.30 ^{+0.11} _{-0.11}		156.83 ^{+380.56} _{-56.00}	52.15 ± 0.04	1, 4
121128A	12.90 ± 0.40	2.2	-0.80 ^{+0.07} _{-0.07}	-2.41 ^{+0.06} _{-0.06}	62.00 ^{+3.02} _{-3.02}	52.79 ± 0.01	1, 3
121201A	0.80 ± 0.10	3.385	-1.85 ^{+0.18} _{-0.19}		54.88 ^{+202.37} _{-32.70}	52.15 ± 0.05	1, 4
121209A	3.40 ± 0.30	2.1	-1.43 ^{+0.08} _{-0.08}		159.35	52.24 ± 0.04	1, 3
121211A	1.00 ± 0.30	1.023	-0.27 ^{+0.37} _{-0.37}		100.00 ^{+15.00} _{-15.00}	50.80 ± 0.13	1, 3
121229A	0.10 ± 0.00	2.707	-2.43 ^{+0.46} _{-0.46}		250.00*	51.53 ± 0.00	2, 3
130131B	1.00 ± 0.20	2.539	-1.24 ^{+0.22} _{-0.22}		300.42 ^{+552.02} _{-188.93}	52.06 ± 0.09	1, 4
130215A	2.50 ± 0.70	0.597	-1.19 ^{+0.11} _{-0.11}	-1.59 ^{+0.04} _{-0.04}	257.00 ^{+130.00} _{-130.00}	51.37 ± 0.12	1, 3
130408A	4.90 ± 1.00	3.757	-0.40 ^{+0.20} _{-0.20}	-2.30 ^{+0.20} _{-0.20}	211.00 ^{+29.00} _{-29.00}	53.33 ± 0.09	1, 3
130418A	0.60 ± 0.20	1.218	0.27 ^{+1.88} _{-1.42}		33.88 ^{+4.70} _{-6.28}	50.51 ± 0.14	1, 4
130420A	3.40 ± 0.20	1.297	-1.52 ^{+0.15} _{-0.15}		33.20 ^{+4.11} _{-4.11}	51.58 ± 0.03	1, 3
130427A	331.00 ± 4.60	0.3399	-0.91 ^{+0.01} _{-0.01}	-3.18 ^{+0.03} _{-0.03}	877.80 ^{+4.90} _{-4.90}	53.00 ± 0.01	1, 3
130427B	3.00 ± 0.40	2.78	-1.64 ^{+0.15} _{-0.15}		102.12	52.46 ± 0.06	1, 3
130505A	30.00 ± 3.10	2.27	-0.81 ^{+0.12} _{-0.11}		738.91 ^{+1073.10} _{-401.76}	53.92 ± 0.04	1, 4
130511A	1.30 ± 0.20	1.3033	-1.54 ^{+0.33} _{-0.34}		149.18 ^{+614.92} _{-93.67}	51.31 ± 0.07	1, 4
130514A	2.80 ± 0.30	3.6	-1.44 ^{+0.17} _{-0.15}		23.91 ^{+9.13} _{-4.57}	52.57 ± 0.05	1, 3
130528A	3.00 ± 0.20	1.25	-1.08 ^{+0.05} _{-0.05}	-2.60 ^{+0.30} _{-0.30}	122.00 ^{+7.00} _{-7.00}	51.65 ± 0.03	3, 3
130604A	0.80 ± 0.20	1.06	-1.65 ^{+0.15} _{-0.15}		105.13 ^{+511.35} _{-35.06}	50.86 ± 0.11	1, 4
130606A	2.60 ± 0.20	5.913	-1.14 ^{+0.15} _{-0.15}		294.00 ^{+90.00} _{-50.00}	53.36 ± 0.03	1, 3
130610A	1.70 ± 0.20	2.092	-1.58 ^{+0.08} _{-0.08}		271.00 ^{+111.00} _{-111.00}	52.04 ± 0.05	1, 3
130612A	1.70 ± 0.30	2.006	-1.01 ^{+2.14} _{-2.14}	-2.23 ^{+0.15} _{-0.15}	26.40 ^{+6.80} _{-6.80}	51.83 ± 0.08	1, 3
130701A	17.10 ± 0.70	1.155	-1.10 ^{+0.06} _{-0.06}		89.00 ^{+2.42} _{-2.42}	52.16 ± 0.02	1, 3
130831A	13.60 ± 0.60	0.4791	-0.61 ^{+0.06} _{-0.06}	-2.30 ^{+0.30} _{-0.30}	55.00 ^{+4.00} _{-4.00}	51.23 ± 0.02	1, 3
130907A	25.60 ± 0.50	1.238	-0.91 ^{+0.02} _{-0.02}	-2.34 ^{+0.07} _{-0.07}	79.50 ^{+4.96} _{-4.96}	52.55 ± 0.01	1, 3
130925A	7.30 ± 0.60	0.347	-1.50 ^{+0.03} _{-0.03}		107.00 ^{+1.81} _{-1.81}	50.60 ± 0.04	2, 3
131030A	28.10 ± 0.70	1.295	-0.71 ^{+0.12} _{-0.12}	-2.95 ^{+0.28} _{-0.28}	177.00 ^{+10.00} _{-10.00}	52.76 ± 0.01	1, 3
131103A	1.50 ± 0.30	0.599	-1.85 ^{+0.37} _{-0.40}		40.66 ^{+224.16} _{-39.66}	50.52 ± 0.09	1, 4
131105A	3.50 ± 0.60	1.686	-1.26 ^{+0.02} _{-0.02}	-2.33 ^{+0.33} _{-0.33}	265.00 ^{+17.00} _{-17.00}	52.23 ± 0.07	1, 3
131117A	0.70 ± 0.10	4.042	-0.17 ^{+1.61} _{-1.10}		44.40 ^{+10.40} _{-6.00}	51.90 ± 0.06	1, 3
131227A	1.10 ± 0.20	5.3	-1.39 ^{+0.13} _{-0.13}		182.21 ^{+527.61} _{-74.11}	52.74 ± 0.08	1, 4
140114A	0.90 ± 0.10	3	-2.06 ^{+0.09} _{-0.09}		250.00*	52.27 ± 0.05	1, 3
140206A	19.40 ± 0.50	2.73	-0.20 ^{+0.06} _{-0.06}	-2.40 ^{+0.06} _{-0.06}	120.00 ^{+3.63} _{-3.63}	53.40 ± 0.01	1, 3
140213A	23.50 ± 0.80	1.2076	-1.13 ^{+0.03} _{-0.03}	-2.26 ^{+0.05} _{-0.05}	86.60 ^{+3.60} _{-3.60}	52.52 ± 0.01	1, 3
140301A	0.70 ± 0.20	1.416	-1.00*	-2.14 ^{+0.36} _{-0.42}	1.01 ^{+31.81} _{-0.02}	51.33 ± 0.12	1, 4
140304A	1.70 ± 0.20	5.283	-0.80 ^{+0.22} _{-0.22}	-2.35 ^{+0.43} _{-0.43}	123.00 ^{+27.00} _{-27.00}	52.95 ± 0.05	1, 3
140311A	1.30 ± 0.50	4.954	-1.62 ^{+0.24} _{-0.24}		77.88 ^{+250.45} _{-27.47}	52.67 ± 0.17	1, 4
140318A	0.50 ± 0.20	1.02	-1.35 ^{+0.29} _{-0.29}		128.40 ^{+434.15} _{-60.53}	50.58 ± 0.17	1, 4
140419A	4.90 ± 0.20	3.956	-0.63 ^{+0.36} _{-0.22}	-2.30 ^{+0.40} _{-2.50}	293.00 ^{+84.00} _{-84.00}	53.45 ± 0.02	1, 3
140423A	2.10 ± 0.20	3.26	-0.58 ^{+0.12} _{-0.12}	-1.83 ^{+0.05} _{-0.05}	121.00 ^{+15.00} _{-15.00}	52.79 ± 0.04	1, 3
140428A	0.60 ± 0.20	4.7	-1.54 ^{+0.26} _{-0.26}		250.00*	52.41 ± 0.14	1, 3
140430A	2.50 ± 0.20	1.6	-1.00*	-2.03 ^{+0.25} _{-0.27}	12.25 ^{+28.12} _{-11.25}	51.90 ± 0.03	1, 4
140506A	10.90 ± 0.90	0.889	-1.18 ^{+0.11} _{-0.11}	-2.30 ^{+0.40} _{-7.70}	197.00 ^{+32.00} _{-32.00}	52.01 ± 0.04	1, 3
140509A	1.60 ± 0.40	2.4	-1.69 ^{+0.21} _{-0.21}		74.08 ^{+242.97} _{-25.89}	52.02 ± 0.11	1, 4
140512A	6.80 ± 0.30	0.725	-1.22 ^{+0.02} _{-0.02}	-3.20 ^{+1.60} _{-1.60}	682.00 ^{+70.00} _{-70.00}	51.82 ± 0.02	1, 3
140515A	0.90 ± 0.10	6.32	-0.98 ^{+0.39} _{-0.39}		51.30 ^{+8.89} _{-8.89}	52.56 ± 0.05	1, 3
140518A	1.00 ± 0.10	4.707	-0.92 ^{+0.37} _{-0.37}		43.90 ^{+4.60} _{-4.60}	52.28 ± 0.04	1, 3
140629A	4.20 ± 0.40	2.275	-1.42 ^{+0.54} _{-0.54}		86.01 ^{+17.53} _{-17.53}	52.32 ± 0.04	1, 3
140703A	2.80 ± 0.60	3.14	-1.10 ^{+0.06} _{-0.06}		177.00 ^{+14.01} _{-14.01}	52.60 ± 0.09	1, 3
140710A	1.90 ± 0.30	0.558				50.87 ± 0.07	1, 3
140907A	2.50 ± 0.20	1.21	-0.97 ^{+0.08} _{-0.08}		113.00 ^{+7.00} _{-7.00}	51.42 ± 0.03	1, 5
141004A	6.10 ± 0.30	0.573	-1.30 ^{+0.10} _{-0.10}		147.00 ^{+28.00} _{-28.00}	51.08 ± 0.02	1, 6

GRB	Peak flux (photons cm ⁻² s ⁻¹)	z	α	β	E_p (keV)	$\log L$ (erg s ⁻¹)	Refs.
141026A	0.40 ± 0.20	3.35	-1.00*	-2.35 ^{+0.21} _{-0.22}	12.25 ^{+8.67} _{-11.25}	51.77 ± 0.22	1, 4
141109A	2.50 ± 0.20	2.993	-1.56 ^{+0.07} _{-0.07}		134.99 ^{+348.35} _{-37.51}	52.47 ± 0.03	1, 4
141121A	0.90 ± 0.30	1.47	-1.79 ^{+0.15} _{-0.15}		60.65 ^{+58.07} _{-18.24}	51.27 ± 0.14	1, 4
141220A	8.90 ± 0.70	1.3195	-0.80 ^{+0.03} _{-0.03}		180.00 ^{+5.44} _{-5.44}	52.21 ± 0.03	1, 3
141221A	3.10 ± 0.20	1.452	-1.07 ^{+0.13} _{-0.13}		152.40 ^{+28.50} _{-28.50}	51.79 ± 0.03	1, 7
141225A	1.30 ± 0.40	0.915	-1.29 ^{+0.16} _{-0.15}		300.42 ^{+552.02} _{-174.05}	51.08 ± 0.13	1, 4
150120B	1.20 ± 0.20	3.5	-1.43 ^{+0.28} _{-0.24}		130.00 ^{+150.00} _{-50.00}	52.29 ± 0.07	1, 8
150206A	10.10 ± 0.40	2.087	-1.20 ^{+0.23} _{-0.22}		189.51 ^{+1157.45} _{-66.47}	52.74 ± 0.02	1, 4
150301B	3.00 ± 0.20	1.5169	-1.50 ^{+0.07} _{-0.07}		149.18 ^{+369.54} _{-47.29}	51.83 ± 0.03	1, 4
150314A	38.50 ± 0.90	1.758	-0.87 ^{+0.12} _{-0.12}		358.71 ^{+381.85} _{-108.15}	53.41 ± 0.01	1, 4
150323A	5.40 ± 0.30	0.593	-1.41 ^{+0.35} _{-0.32}		81.38 ^{+176.78} _{-17.78}	50.97 ± 0.02	1, 4
150403A	17.60	2.06	-0.96 ^{+0.16} _{-0.15}		227.86 ^{+189.81} _{-59.89}	53.05 ± 0.00	1, 4
150413A	1.60 ± 0.30	3.139	-1.72 ^{+0.14} _{-0.14}		77.88 ^{+195.76} _{-21.93}	52.32 ± 0.08	1, 4
150727A	1.00 ± 0.20	0.313	-0.89 ^{+0.41} _{-0.37}		152.40 ^{+1257.81} _{-51.73}	49.69 ± 0.09	1, 4
150818A	2.40 ± 0.30	0.282	-1.86 ^{+0.10} _{-0.10}		74.08 ^{+825.80} _{-68.05}	49.99 ± 0.05	1, 4
150910A	1.10 ± 0.40	1.359	-1.43 ^{+0.14} _{-0.13}		271.83 ^{+522.06} _{-169.04}	51.39 ± 0.16	1, 4
150915A	0.50 ± 0.20	1.968				51.60 ± 0.17	1, 3
151021A	9.70 ± 0.80	2.33	-1.14 ^{+0.15} _{-0.14}	-2.46 ^{+0.18} _{-0.32}	170.00 ^{+23.00} _{-18.00}	52.91 ± 0.04	1, 9
151027A	6.80 ± 0.60	0.81	-1.14 ^{+0.04} _{-0.04}		340.00 ^{+63.00} _{-63.00}	51.73 ± 0.04	1, 3
151029A	1.80 ± 0.30	1.423	-0.86 ^{+1.18} _{-0.95}		31.34 ^{+7.13} _{-17.25}	51.26 ± 0.07	1, 4
151031A	1.70 ± 0.20	1.167				51.59 ± 0.05	1, 3
151111A	1.00 ± 0.10	3.5	-0.12 ^{+5.12} _{-0.82}	-2.32 ^{+0.32} _{-0.59}	45.22 ^{+0.03} _{-0.47}	52.13 ± 0.04	1, 4
151112A	1.90 ± 0.20	4.1	-1.87 ^{+0.17} _{-0.17}		49.66 ^{+34.95} _{-22.08}	52.74 ± 0.05	1, 4
151215A	1.60 ± 0.20	2.59				52.39 ± 0.05	1, 3
160121A	1.20 ± 0.20	1.96				51.98 ± 0.07	1, 3
160131A	6.40 ± 0.30	0.972	-1.22 ^{+0.04} _{-0.04}		385.74 ^{+632.85} _{-142.71}	51.92 ± 0.02	1, 4
160203A	1.30 ± 0.40	3.52				52.60 ± 0.13	1, 3
160227A	0.60 ± 0.10	2.38				51.87 ± 0.07	1, 3
160228A	1.20 ± 0.10	1.64				51.79 ± 0.04	1, 3
160314A	0.90 ± 0.20	0.726				50.82 ± 0.10	1, 3
160327A	1.80 ± 0.20	5?				53.08 ± 0.05	1, 3
160410A	3.50 ± 0.30	1.717	-0.82 ^{+0.14} _{-0.14}		495.30 ^{+890.16} _{-232.98}	52.50 ± 0.04	2, 4
160425A	2.80 ± 0.20	0.555				51.03 ± 0.03	1,
160804A	2.90 ± 0.30	0.736	-1.10 ^{+0.10} _{-0.10}		74.00 ^{+3.00} _{-3.00}	50.87 ± 0.04	1, 10
161014A	2.90 ± 0.60	2.823	-1.57 ^{+0.16} _{-0.16}		110.52 ^{+309.25} _{-41.46}	52.45 ± 0.09	1, 4
161017A	2.80 ± 0.20	2.013	-1.25 ^{+0.16} _{-0.16}		289.00 ^{+73.00} _{-73.00}	52.25 ± 0.03	1, 11
161108A	0.60 ± 0.10	1.159				51.13 ± 0.07	1,
161117A	6.80 ± 0.30	1.549	-0.43 ^{+0.07} _{-0.07}	-2.27 ^{+0.04} _{-0.04}	68.04 ^{+2.66} _{-2.66}	52.22 ± 0.02	1, 12
161129A	3.40 ± 0.20	0.645	-1.29 ^{+0.25} _{-0.24}		128.54 ^{+266.70} _{-35.78}	50.92 ± 0.03	1, 4
161219B	5.30 ± 0.40	0.1475	-1.59 ^{+0.71} _{-0.71}		91.00 ^{+21.00} _{-21.00}	49.62 ± 0.03	1, 13
170113A	1.10 ± 0.10	1.968	-0.75 ^{+0.59} _{-0.59}		73.30 ^{+33.60} _{-33.60}	51.47 ± 0.04	1, 14
170202A	4.70 ± 0.30	3.645	-1.16 ^{+0.59} _{-0.34}		247.00 ^{+166.00} _{-86.00}	53.07 ± 0.03	1, 15
170519A	0.70 ± 0.10	0.818				50.83 ± 0.06	1,
170531B	0.80 ± 0.20	2.366				51.99 ± 0.11	1,
170604A	4.20 ± 0.90	1.329	-1.40 ^{+0.13} _{-0.12}		245.96 ^{+621.09} _{-115.66}	51.93 ± 0.09	1, 4
170705A	13.90 ± 0.40	2.01	-0.88 ^{+0.07} _{-0.07}	-2.38 ^{+0.09} _{-0.09}	100.00 ^{+10.00} _{-10.00}	52.83 ± 0.01	1, 16
170903A	3.90 ± 0.50	0.886				51.66 ± 0.06	1,
171020A	0.70 ± 0.20	1.87				51.70 ± 0.12	1,
171222A	0.70 ± 0.20	2.409	-1.09 ^{+0.27} _{-0.27}		29.18 ^{+2.73} _{-2.73}	51.45 ± 0.12	1, 17
180115A	0.60 ± 0.20	2.487?				51.92 ± 0.14	1,
180205A	3.40 ± 0.30	1.409	-1.38 ^{+0.15} _{-0.15}		85.00 ^{+14.40} _{-14.40}	51.70 ± 0.04	1, 18
180314A	7.90 ± 0.60	1.445	-0.61 ^{+0.17} _{-0.16}		111.00 ^{+6.00} _{-6.00}	52.10 ± 0.03	2, 19
180325A	9.40 ± 0.30	2.248	-0.50 ^{+0.21} _{-0.19}	-2.65 ^{+0.31} _{-1.06}	306.00 ^{+50.00} _{-39.00}	53.18 ± 0.01	1, 20
180329B	1.40 ± 0.40	1.998	-0.97 ^{+0.56} _{-0.56}		48.60 ^{+9.10} _{-9.10}	51.55 ± 0.12	1, 21
180404A	1.30 ± 0.20	1				51.31 ± 0.07	1,
180510B	1.20 ± 0.20	1.305				51.56 ± 0.07	1,
180620B	3.60 ± 0.20	1.1175	-0.50 ^{+0.20} _{-0.20}	-2.20 ^{+0.10} _{-0.10}	106.00 ^{+15.00} _{-15.00}	51.74 ± 0.02	1, 22
180624A	1.40 ± 0.20	2.855	-1.89 ^{+0.10} _{-0.10}		54.88 ^{+360.57} _{-47.74}	52.24 ± 0.06	1, 4
180728A	132.00 ± 2.90	0.117	-1.54 ^{+0.02} _{-0.01}	-2.46 ^{+0.02} _{-0.02}	79.20 ^{+1.40} _{-1.40}	50.86 ± 0.01	1, 23

GRB	Peak flux (photons cm ⁻² s ⁻¹)	z	α	β	E_p (keV)	$\log L$ (erg s ⁻¹)	Refs.
181010A	1.40 ± 0.20	1.39	$-0.80^{+0.20}_{-0.20}$		$280.00^{+80.00}_{-80.00}$	51.64 ± 0.06	1, 24
181020A	7.70 ± 0.30	2.938	$-0.73^{+0.13}_{-0.11}$	$-2.35^{+0.22}_{-0.41}$	$371.00^{+57.00}_{-52.00}$	53.41 ± 0.02	1, 25
181110A	3.70 ± 0.30	1.505	$-1.63^{+0.34}_{-0.26}$		$48.00^{+14.00}_{-27.00}$	51.83 ± 0.04	1, 26
190106A	5.50 ± 0.30	1.859	$-1.00^{+0.63}_{-0.50}$		$171.00^{+90.00}_{-42.00}$	52.34 ± 0.02	1, 27
190114A	0.50 ± 0.20	3.3765				52.15 ± 0.17	1,
190114C	101.00 ± 1.50	0.425	$-1.06^{+0.00}_{-0.00}$	$-3.18^{+0.07}_{-0.07}$	$998.60^{+11.90}_{-11.90}$	52.66 ± 0.01	1, 28
190324A	11.90 ± 0.50	1.1715	$-0.84^{+0.04}_{-0.04}$	$-2.06^{+0.05}_{-0.05}$	$144.30^{+8.40}_{-8.40}$	52.41 ± 0.02	2, 29
190613A	1.50 ± 0.70	2.78?	$0.06^{+0.18}_{-0.18}$		$108.00^{+5.00}_{-5.00}$	52.08 ± 0.20	1, 30
190719C	5.50 ± 0.30	2.469	$-0.87^{+0.18}_{-0.18}$		$81.00^{+9.00}_{-9.00}$	52.44 ± 0.02	1, 31
190829A	18.00 ± 2.70	0.0785	$-1.33^{+0.30}_{-0.23}$		$579.00^{+2282.00}_{-281.00}$	49.94 ± 0.07	1, 32
191004B	5.00 ± 0.20	3.503	$-0.51^{+0.34}_{-0.30}$		$172.00^{+27.00}_{-21.00}$	53.01 ± 0.02	2, 33
191011A	1.80 ± 0.20	1.722	$-1.24^{+0.29}_{-0.29}$		$89.00^{+23.00}_{-23.00}$	51.62 ± 0.05	2, 34
191019A	5.70 ± 0.40	0.248				50.53 ± 0.03	2,

Note. Columns show, in order, the GRB name; the peak photon flux in the 15–150 keV *Swift*/BAT energy band (with 90% confidence level error); the redshift; various spectral parameters (with 68% confidence level errors), including the low-energy photon index α , the high-energy photon index β , and the observer-frame peak energy E_p ; and the peak bolometric luminosity in units of erg s⁻¹ (calculated in the 1–10⁴ rest-frame energy range, with 90% confidence level error that propagated from the error of the peak flux only). (*) Bursts with missing α or E_p are reported with the typical values of -1 or 250 keV. In the last column, we give the references, in order, for the redshift and for the spectral parameters: 1) <https://www.mpe.mpg.de/jcg/grbgen.html>; 2) <https://swift.gsfc.nasa.gov/archive/grbtable/>; 3) Wang et al. (2020); 4) Butler et al. (2007); 5) Zhang (2014); 6) Pelassa (2014); 7) Yu (2014); 8) von Kienlin & Burns (2015); 9) Golenetskii et al. (2015); 10) Bissaldi et al. (2016); 11) Frederiks et al. (2016a); 12) Mailyan & Goldstein (2016); 13) Frederiks et al. (2016b); 14) Markwardt et al. (2017); 15) Frederiks et al. (2017); 16) Bissaldi & Meegan (2017); 17) Stanbro et al. (2017); 18) von Kienlin (2018a); 19) Tsvetkova et al. (2018a); 20) Frederiks et al. (2018a); 21) Palmer et al. (2018); 22) Mailyan (2018); 23) Veres et al. (2018); 24) von Kienlin (2018b); 25) Tsvetkova et al. (2018b); 26) Frederiks et al. (2018b); 27) Tsvetkova et al. (2019a); 28) Hamburg et al. (2019); 29) Hui (2019); 30) Poolakkil et al. (2019a); 31) Poolakkil et al. (2019b); 32) Tsvetkova et al. (2019b); 33) Svinkin et al. (2019); 34) Bissaldi et al. (2019).

This paper has been typeset from a TeX/LaTeX file prepared by the author.